A PRELIMINARY STUDY OF FLOTATION DEINKING MODEL VALIDATION

Project F00903

Report 9

to the

MEMBER COMPANIES OF THE INSTITUTE OF PAPER SCIENCE AND TECHNOLOGY

August 1999

INSTITUTE OF PAPER SCIENCE AND TECHNOLOGY

Atlanta, Georgia

A PRELIMINARY STUDY OF FLOTATION DEINKING MODEL VALIDATION

Project F00903

Report 9

A Progress Report

to the

MEMBER COMPANIES OF THE INSTITUTE OF PAPER SCIENCE AND TECHNOLOGY

By

T.J. Heindel, F. Bloom, and A.E. Garner

August 1999

TABLE OF CONTENTS

1 EXECUTIVE SUMMARY 1

2 INTRODUCTION 1

3 MATHEMATICAL MODEL 2

3.1 Model Equation Review 2

3.2 Update of Z and Z' 8

3.2.1 The Bubble/Particle Attachment Frequency (Z) 9

3.2.1.1 Z_{12} Without Particle Body Forces 11

3.2.1.2 Z_{12} With Particle Body Forces 13

3.2.2 The Bubble/Particle Detachment Frequency (Z') 15

3.3 The Semi-Batch Process Model 17

3.3.1 Short-Time Solution 17

3.3.2 Low Gas Holdup Solution 20

3.4 Model Summary 23

4 EXPERIMENTAL PROCEDURES 26

4.1 Model Flotation Cell 27

4.2 Stock Preparation 27

4.2.1 Toner Particle Generation 27

4.2.2 Fiber/Toner Mixture 27

4.3 Experimental Conditions 28

4.4 Data Analysis 29

4.4.1 Surface Tension Measurements 29

4.4.2 Handsheet Preparation 29

4.4.3 Image Analysis 29

5 RESULTS 30
5.1 Experimental Results 30
5.2 Comparisons to Model Predictions 32
5.3 Discrepancy Explanation 35
5.3.1 Experimental 35
5.3.2 Theoretical 35
5.4 Limited Parametric Studies 36
5.4.1 Effect of Surface Tension 36
5.4.2 Effect of the Surface Mobility Coefficient 37
5.4.3 Effect of the Initial-to-Critical Film Thickness 37
6 CONCLUSIONS 38
7 FUTURE WORK 38
8 NOMENCLATURE LIST 40
9 REFERENCES 46
10 TABLES 49
11 FIGURES 51
12 APPENDIX 67

1 EXECUTIVE SUMMARY

This report summarizes the current flotation model, which incorporates the various microprocesses typically associated with flotation separation. The model is then applied to a semi-batch flotation process, approximating laboratory conditions. Laboratory flotation data are also obtained to compare predicted flotation efficiencies with experimentally determined values. It was shown that the predictions did not match the experimental results very well.

The discrepancy between the theoretical predictions and the experimental values was the result of two primary shortcomings. First, the experimental flotation cell did not supply enough mixing to evaluate the possible destabilization of the bubble/particle aggregate. Second, the theoretical model was originally derived assuming that only one particle can attach to a bubble. Both of these shortcomings over-simplified the actual flotation process and caused discrepancies in the observed results.

Research is currently being conducted to remove the shortcomings identified above. This includes using a standard laboratory flotation cell, which creates a significant amount of mixing, in the validation experiments, as well as allowing for more than one particle to attach to a bubble in the theoretical model.

2 INTRODUCTION

Flotation deinking is a common unit operation used in the paper industry to remove hydrophobic contaminant particles (i.e., inks, toners, etc.) from cellulose fiber suspensions. A recent summary of the fundamentals of this process has been presented by Heindel [1999]. Although much research has been completed in this area, the current level of understanding is insufficient for complete process optimization. The goal of this research effort is to develop a model of the flotation deinking process that can be used in the optimization of current flotation technology and in the development of new (improved) technology.

This effort began by reviewing the current technology, which is commonly divided into

a series of microprocesses. A two-parameter population balance-type kinetic model of the overall macroprocess was then proposed based on the microprocesses. This has been summarized in Report 1 of this project [Heindel and Bloom, 1995]. Predictions based on the initial model have been presented in Report 2 of this project [Heindel and Bloom, 1996]. Report 4 [Heindel and Bloom, 1998a] and 6 [Heindel and Bloom, 1998b] of this project revisited the microprocesses of collision and attachment by sliding, respectively, and provided improved probabilities that these microprocesses will successfully occur. Report 7 of this project [Maruvada and Heindel, 1998] provided an initial methodology for validating our flotation model. This current report improves upon the model validation procedures and presents initial flotation model validation data. Discrepancies between the data and model are also summarized in this report. Finally, experimental validation and theoretical model improvements are also highlighted. (Note that Reports 3 [Heindel, 1997], 5 [Heindel and Emery, 1998], and 8 [Heindel and Garner, 1999] of this project involve bubble size visualization and measurement results, which will be incorporated into the modeling aspects of this project when the time comes.)

3 MATHEMATICAL MODEL

The flotation model employed in this study is summarized below. This includes previously described improvements to our model, as well as new improvements to the collision "frequencies" (Z and Z'). The extension to a semi-batch process which is used in the model validation is also highlighted.

3.1 Model Equation Review

In this section we recall the system of equations developed by Maruvada and Heindel [1998] for the semi-batch flotation process; the model in question represents a special case of the earlier work presented in Report 1 [Heindel and Bloom, 1995]. In all the work referenced above it is assumed that the bubbles and particles are spherical and uniform in size and that

only one particle can attach to a given bubble.

The experimental apparatus to which the model described below applies consists of a column into which a desired furnish is loaded and a sparger at the bottom for air supply. Air at a known, constant, volumetric flow rate (Q), is bubbled through the suspension containing the recycled cellulose fibers and ink particles. It is assumed that air bubbles that are formed at the bottom of the column rise through the suspension at their terminal rise velocity. Bubble coalescence is assumed to be negligible and the entire bubble surface is assumed to be rigid because of the presence of surface active substances; this is a valid assumption as long as the bubble size is small. In the assumed semi-batch process a fixed volume of the pulp suspension is used while air is continuously injected. The experimental system is indicated in Fig. 1. The mixture volume (including stock and gas) in a steady state situation is denoted by V. The agitator provides the agitation necessary for bubble/particle mixing.

Assuming that all bubbles have a uniform size, the number of bubbles in the column can be calculated by measuring the gas holdup and the size of an individual bubble. The total number of bubbles consists of bubbles free of particles and those with particles attached to them. Both the free bubble concentration (n_B^f) and the bubbles with particles attached (n_B^a) are functions of time, while the concentration of bubbles is a constant, n_B, at any given instant of time:

$$n_B = n_B^f(t) + n_B^a(t) \tag{3.1}$$

If V_B is the volume of a single bubble, then the total number of air bubbles entering the column per unit time is

$$\dot{N}_B = \frac{Q}{V_B} \tag{3.2}$$

The superficial gas velocity is defined as the volumetric gas flow rate divided by the column cross-sectional area, i.e.,

$$v_g = \frac{Q}{A_c} \tag{3.3}$$

Since Q and A_c are easily measured and controlled, the superficial gas velocity can be

specified in any experiment. This parameter is used to define a characteristic time

$$t^* \equiv \frac{H}{v_g} = \frac{HA_c}{Q} = \frac{V}{Q} \tag{3.4}$$

which is the time required for the gas to replace one column volume.

Assuming negligible bubble coalescence, under steady-state conditions the total number of bubbles entering the column is identical with the total number of bubbles leaving the column. We let n_B^a/n_B denote the fraction of bubbles with particles attached inside the column. As the contents of the column are assumed to be well mixed, the same fraction also represents the fraction of bubbles with attached particles in the exit stream. Assuming that each bubble with attached particles is carrying only one ink particle, the number of ink particles leaving the column can be calculated by multiplying this fraction with the total number of bubbles leaving the column. Hence, the rate of decrease of the ink particles inside the column is given by

$$V\frac{dn_p}{dt} = -\frac{Q}{V_B n_B}(n_p - n_p^f) \tag{3.5}$$

where n_p and n_p^f, which are both functions of time, are the total number of particles per unit volume and the number of free particles per unit volume available to attach to free bubbles, respectively.

Another balance equation can be written for the concentration of free particles inside the column. We note that no free ink particles are either entering or leaving the column and they are only participating in the formation of bubble/particle aggregates. Using the two-parameter kinetic model previously detailed in Report 1 [Heindel and Bloom, 1995], the balance equation for the concentration of free ink particles has the form

$$\frac{dn_p^f}{dt} = -k_1 n_p^f n_B^f + k_2 n_B^a \tag{3.6}$$

In (3.6) k_1 and k_2 are the rate constants for the forward and reverse reactions respectively; these two constants depend upon the various microprocess probabilities that comprise the mechanism of bubble/particle aggregate formation and destruction and are functions of the

bubble, particle, fluid, and system properties. Specifically, the rate constants are given by

$$k_1 = Z P_c P_{asl} P_{tpc} P_{stab} \tag{3.7a}$$

$$k_2 = Z' P_{destab} = Z'(1 - P_{stab}) \tag{3.7b}$$

where Z is the collision frequency between the particles and bubbles, P_c is the probability of collision between a particle and bubble, P_{asl} is the probability of adhesion by sliding, P_{tpc} is the probability of three-phase contact, P_{stab} is the probability of stability of a bubble/particle aggregate, P_{destab} is the probability of destabilization of a bubble/particle aggregate, and Z' is the detachment frequency of particles from bubbles. Updated expressions for the frequencies Z and Z' are developed in this report in Section 3.2. The probability of the formation of a three-phase contact between a liquid, bubble, and particle has been shown to be nearly 1 over a wide range of parameters Schulze [1993, 1994] and will be specified to be exactly 1 in this report, i.e., $P_{tpc} = 1.0$.

The probability of stability, P_{stab}, addresses the stabilization/destabilization of a bubble/particle aggregate. According to Schulze [1993], a reasonable form for P_{stab} is

$$P_{stab} = 1 - \exp\left(1 - \frac{1}{Bo'}\right) \tag{3.8}$$

where the modified Bond number (Bo') is defined as the ratio of detachment to attachment forces, i.e.,

$$Bo' = \frac{F_{\text{detachment}}}{F_{\text{attachment}}} = \frac{4R_p^2\left(\Delta\rho_l g + \dfrac{1.9\rho_p \epsilon^{2/3}}{(R_p + R_B)^{1/3}}\right) + 3R_p\left(\dfrac{2\sigma}{R_B} - 2R_B\rho_l g\right)\sin^2\left(\pi - \dfrac{\theta}{2}\right)}{\left|6\sigma \sin\left(\pi - \dfrac{\theta}{2}\right)\sin\left(\pi + \dfrac{\theta}{2}\right)\right|} \tag{3.9}$$

The various parameters introduced in (3.9) are defined as follows:

$$\begin{cases} R_p & = & \text{the particle radius} \\ R_B & = & \text{the bubble radius} \\ \epsilon & = & \text{the (Kolmogorov) turbulent energy density (or dissipation rate)} \\ g & = & \text{acceleration due to gravity} \\ \sigma & = & \text{the surface tension} \\ \theta & = & \text{the contact angle} \\ \rho_B & = & \text{the bubble (gas) density} \\ \rho_l & = & \text{the fluid density} \\ \rho_p & = & \text{the particle density} \\ \Delta\rho_B & = & \text{the density difference } (\rho_B - \rho_l) \\ \Delta\rho_p & = & \text{the density difference } (\rho_p - \rho_l) \end{cases} \tag{3.10}$$

In our computations we will employ the following relationship among the surface tension, bubble radius, and turbulent energy density to estimate ϵ since σ and R_B are measured [Schulze, 1994]:

$$\sigma = (2R_{B,\max})^{5/3}\epsilon^{2/3}\rho_l \tag{3.11}$$

For the probabilities of collision (P_c) and adhesion by sliding (P_{asl}) we will employ new results which have been developed, respectively, in Heindel and Bloom [1998a, b] for flotation deinking conditions. Beginning with P_c, if $\boldsymbol{v}_p$ represents the particle velocity, and Re_p is the particle Reynolds number

$$Re_p = \frac{2R_p|\boldsymbol{v}_p|}{\nu_l} \tag{3.12}$$

where $\nu_l = \mu_l/\rho_l$ is the kinematic viscosity (μ_l being the dynamic viscosity), then for an intermediate flow about the bubble surface, in which $2 < Re_p < 500$, it follows from the work in Heindel and Bloom [1998a] that

$$P_c = \frac{1}{1+|G|}\left[\frac{1}{2(R_p+R_B)^3}\{2R_p^3 + 3R_p^2R_B\} + \frac{2Re_B^*}{(R_p+R_B)^4}\{R_BR_p^3 + 2R_B^2R_p^2\}\right] + \frac{|G|}{1+|G|} \tag{3.13}$$

In (3.13) G is the dimensionless particle settling velocity, i.e.,

$$G = v_{ps}/v_B \tag{3.14}$$

where v_{ps} is the particle settling velocity and v_B is the bubble (terminal) rise velocity. Also,

$$Re_B^* = \frac{1}{15}Re_B^{0.72} \tag{3.15}$$

where Re_B,

$$Re_B = \frac{2v_B R_B}{\nu_l} \tag{3.16}$$

is the bubble Reynolds number. For the same kind of intermediate flow over the bubble surface (e.g., Yoon and Luttrell [1989]) it follows from recent work of Heindel and Bloom [1998b] that

$$P_{asl} = \exp\left[-2\left(\frac{\lambda}{C_B}\right)\left(\frac{R_p}{R_B+R_p}\right)\left\{\frac{g(R_B+R_p)-G}{|k(R_B+R_p)|-G}\right\}\left(\frac{h_0}{h_{crit}}-1\right)\right] \tag{3.17}$$

where

$$g(r) = \left(1-\frac{3R_B}{r}-\frac{R_B^3}{4r^3}\right)+Re_B^*\left(\frac{R_B}{r}+\frac{R_B^3}{r^3}-\frac{2R_B^4}{r^4}\right) \tag{3.18}$$

and

$$k(r) = -\left\{\left(1-\frac{3R_B}{2r}+\frac{R_B^3}{2r^3}\right)+2Re_B^*\left(\frac{R_B^4}{r^4}-\frac{R_B^3}{r^3}-\frac{R_B^2}{r}+\frac{R_B}{r}\right)\right\} \tag{3.19}$$

while

$$\lambda = 6\pi\mu_l R_p/f \tag{3.20}$$

is the dimensionless friction factor (f the usual fluid flow friction factor). Also, C_B is a parameter which varies between one (for a completely immobilized or rigid bubble surface) and four (for an unrestrained bubble surface), h_0 is the (initial) thickness of the liquid film in the sliding process, and $h_{crit} \leq h_0$ is the film thickness at which the film spontaneously ruptures. The recently derived expressions (3.13) for P_c and (3.17) for P_{asl} will be employed in the computations reported in the present work, i.e., in (3.7a,b).

Since the total number of particles per unit volume can be represented as

$$n_p(t) = n_p^f(t) + n_p^a(t) \tag{3.21}$$

where $n_p^a(t)$ denotes the number of particles per unit volume attached to bubbles at time t (with $n_p^a(t) = n_B^a(t)$ in this report), we may rewrite (3.6) in the form

$$\frac{dn_p^f}{dt} = -k_1 n_p^f n_B + k_1 n_p^f (n_p - n_p^f) + k_2(n_p - n_p^f) \tag{3.22}$$

Equations (3.5) and (3.22) are coupled to each other and must be solved, simultaneously, subject to the initial condition that $n_p(0) = n_p^f(0) = n_{po}^f$, where n_{po}^f is the number density of free ink particles at time $t = 0$. The governing equations can be non-dimensionalized by noting that

$$n_p, n_p^f \sim n_{po}^f \qquad k_1 \sim \left(t^* n_{po}^f\right)^{-1}$$

$$t \sim t^* (= V/Q) \qquad k_2 \sim (t^*)^{-1}$$

Once a bubble reaches the froth layer, it is assumed to be removed from the system. The new dimensionless variables are

$$\begin{aligned} \alpha = n_p/n_{po}^f, \gamma = n_p^f/n_{po}^f \qquad & \tilde{k}_1 = k_1 t^* n_{po}^f \\ \tilde{t} = t/t^* \qquad & \tilde{k}_2 = k_2 t^* \end{aligned} \tag{3.23}$$

Using the above scheme, the two governing equations, (3.5) and (3.22), with the accompanying initial conditions, may be scaled and rewritten as follows:

$$\epsilon_p \alpha' = -(\alpha - \gamma); \;\; \alpha(\tilde{t} = 0) = 1 \tag{3.24a}$$

$$\gamma' = -\tilde{k}_1 E \gamma + \tilde{k}_1 \gamma(\alpha - \gamma) + \tilde{k}_2(\alpha - \gamma); \;\; \gamma(\tilde{t} = 0) = 1 \tag{3.24b}$$

In (3.24a,b) the prime indicates differentiation with respect to dimensionless time. The two parameters that appear in the scaled equations are $\epsilon_p = V_B n_B$ and $E = n_B/n_{po}^f$, where ϵ_p is the gas holdup per unit volume and E is a measure of the relative bubble population with respect to the initial number of ink particles.

The system of equations (3.24a, b) will be the starting point for the analysis of the semi-batch process model in Section 3.3.

3.2 Update of Z and Z'

In this section we obtain new expressions, specific to flotation deinking fluid mechanics, for the 'frequencies' Z and Z' which appear in the definitions of the kinetic constants k_1 and k_2 (i.e., in (3.7a,b)). We note that, in (3.7a,b), Z' is a true detachment frequency inasmuch as it will be seen, below, to have the dimensions of t^{-1}; however, it will also be clear, from the

discussion which follows, that Z is not a true frequency because it will have the dimensions L^3t^{-1}. Thus k_2 has dimension t^{-1} while that of k_1 is L^3t^{-1}. Each of the three distinct terms in (3.6) has the dimension of number/volume-time.

3.2.1 The Bubble/Particle Attachment Frequency (Z)

Many different expressions have appeared in the literature for the attachment 'frequency' associated with the interaction of particles in a moving fluid; among the best known of these are the results attributed to Smoluchowski [1917], i.e.,

$$Z_{12} = 4/3 N_1 N_2 d_{12}^3 \bar{G} \tag{3.25}$$

where N_i is the number of particles of species i per unit volume ($i = 1, 2$), $d_{12} = R_1 + R_2$ is the sum of the radii of particles associated with the two distinct species, and $\bar{G}$ is the velocity gradient perpendicular to the direction of motion of the particles. The expression (3.25) assumes a suspension of particles in a fluid moving under uniform shear with the particles being randomly distributed and following, up to the moment of impact, the fluid streamlines as if no other particles were present.

For turbulent flows, Camp and Stein [1943] applied (3.25) with $\bar{G}$ replaced by the mean velocity gradient $\bar{G} = (\epsilon/\nu_l)^{1/2}$; thus

$$Z_{12} = \frac{4}{3} N_1 N_2 d_{12}^3 (\epsilon/\nu_l)^{1/2} \tag{3.26}$$

Saffman and Turner [1956] obtained a result similar to (3.26), the only difference being the replacement of the constant 4/3 in (3.26) by the value $\sqrt{8\pi/15}$. However, results like (3.26) are only valid when d_{12} is small relative to the smallest eddies in the fluid and for particles which completely follow the fluid motion. In particular, results such as (3.26) are based on turbulence with low energy dissipation, with the problem confined within the smallest eddies, and assumes that the particle paths relative to an eddy are fully determined by the eddy fluid velocities and accelerations. Results such as (3.26), therefore, are not valid for larger particles and/or more vigorous fluid turbulence. In large scale industrial situations (e.g.,

commercial flotation deinking tanks) particles will acquire momentum in one or more eddies and then will be projected into a neighboring eddy; such a situation calls for a classical kinetic theory treatment and entails finding an expression for the distribution of particle velocities.

Batchelor [1953] showed that because fluid elements in a turbulent flow are subject to the influence of large numbers of neighboring random eddies, the Central Limit Theorem may be used to predict that the resultant particle velocity distribution should be Gaussian. Thus, if the particle velocity distribution has a mean of zero and a variance $\bar{U}_p^2$ (which is dependent on the particle size) the distribution of velocities for a particle moving in one direction is given by the probability distribution

$$dP = \frac{1}{\sqrt{2\pi\bar{U}_p^2}} \exp\left[\frac{-U_p^2}{2\bar{U}_p^2}\right] dU_p \tag{3.27}$$

which represents the probability of finding the particle with a velocity between U_p and $U_p + dU_p$. The derivation of (3.27) also assumes that the turbulence is in the inertial convection subrange, i.e., that

$$L > \bar{\lambda} > \eta \tag{3.28}$$

where L is the macroscale associated with the turbulent flow, $\eta = (\nu_l^3/\epsilon)^{1/4}$ is the (Kolmogorov) microscale, and $\bar{\lambda}$ is comparable to the eddy size of interest (e.g., a particle, bubble, or aggregate diameter).

In order to employ (3.27) to compute a collision frequency, as we do below, we must assume the independence of colliding particle velocities, both in magnitude and direction; in particular, as noted by Abrahamson [1975], the fluid must be isotropic on the scale of the collision process. The smallest particle diameter d_p for the independent velocity assumption to hold must satisfy

$$d_p^2 > 15\mu_l\bar{U}^2/\rho_p\epsilon \tag{3.29}$$

where $\bar{U}$ is the mean fluid velocity deviation. If we are, indeed, talking about a collision process between two different types of particles then (3.29) must hold for each class of

particle. If, however, we follow the work of Schubert and Bischofberger [1981], and apply the analysis which follows to the case of particle/bubble collisions in a flotation tank, then (3.29) must hold with respect to the (ink) particles and the analogous restriction, i.e.,

$$d_B^2 > 15\mu_l \bar{U}^2/\rho_B \epsilon \tag{3.30}$$

must be satisfied by air bubbles of diameter d_B. As ρ_B is very small it is not immediately clear that (3.30) will be satisfied in any situation of practical interest. That (3.30) is, indeed, reasonable for particle/bubble collisions, in a simple laboratory scale semi-batch process, will be verified once we have completed the derivation of the expression for Z_{12}; this derivation follows the analysis in Abrahamson [1975] and is based directly on the Gaussian probability distribution (3.27) for the particle velocities.

3.2.1.1 Z_{12} Without Particle Body Forces

If we consider two species of particles with concentrations N_1, N_2, velocity distribution variances (i.e., velocities relative to the mean fluid velocity) $\bar{U}_1, \bar{U}_2$, and velocity fields (U_1, V_1, W_1) and (U_2, V_2, W_2), then the concentration dN_1 of particles of the first species, with velocity components in the range U_1 to $U_1 + dU_1$, V_1 to $V_1 + dV_1$, and W_1 to $W_1 + dW_1$ is

$$dN_1 = dP_U dP_V dP_W \tag{3.31}$$

where dP_U, e.g., is given by (3.27) with $U_p = U_1$ and $\bar{U}_p = \bar{U}_1$, while dP_V is given by (3.27) with $U_p = V_1$ and $\bar{U}_p = \bar{U}_1$, and dP_W is given by (3.27) with $U_p = W_1$ and $\bar{U}_p = \bar{U}_1$. Thus, taking into account the particle concentrations

$$dN_1 = \frac{N_1}{(\sqrt{2\pi\bar{U}_1^2})^3} \exp\left[\frac{-(U_1^2 + V_1^2 + W_1^2)}{2\bar{U}_1^2}\right] dU_1 dV_1 dW_1 \tag{3.32}$$

and, in an analogous fashion, for the second species of particles

$$dN_2 = \frac{N_2}{(\sqrt{2\pi\bar{U}_2^2})^3} \exp\left[\frac{-(U_2^2 + V_2^2 + W_2^2)}{2\bar{U}_2^2}\right] dU_2 dV_2 dW_2 \tag{3.33}$$

It we set

$$\mathcal{V}_{12} = (U_1 - U_2)^2 + (V_1 - V_2)^2 + (W_1 - W_2)^2, \tag{3.34}$$

i.e., $\mathcal{V}_{12}$ is the relative velocity between the particles of the two species (or between particles and bubbles for particle/bubble interactions), and set dZ_{12} equal to the number of collisions/volume-time between the two types of particles (within the given velocity intervals) then

$$dZ_{12} = dN_1 dN_2 d_{12}^2 \mathcal{V}_{12} \tag{3.35}$$

Substituting (3.32) - (3.34) into (3.35) and integrating, one obtains as the expression for the total number of collisions per unit volume, per unit time

$$\begin{aligned} Z_{12} &= 2^{3/2}\pi^{1/2} N_1 N_2 d_{12}^2 \sqrt{\bar{U}_1^2 + \bar{U}_2^2} \\ &\simeq 5.0 N_1 N_2 d_{12}^2 \sqrt{\bar{U}_1^2 + \bar{U}_2^2} \end{aligned} \tag{3.36}$$

In applying (3.36) to particle/bubble collisions we must take

$$\left\{ \begin{array}{lcl} d_{12} & = & R_p + R_B \\ \bar{U}_1 & = & \bar{U}_p \;\; \bar{U}_2 = \bar{U}_B \\ N_1 & = & n_p^f, \;\; N_2 = n_B^f \end{array} \right. \tag{3.37}$$

where the effective values of relative velocity between (respectively) particles (bubbles) and the fluid are given by the expressions first delineated in Liepe and Möckel [1976], namely,

$$\bar{U}_p = 0.4 \frac{\epsilon^{4/9} d_p^{7/9}}{\nu_l^{1/3}} \left(\frac{\rho_p - \rho_l}{\rho_l} \right)^{2/3} \tag{3.38a}$$

$$\bar{U}_B = 0.4 \frac{\epsilon^{4/9} d_B^{7/9}}{\nu_l^{1/3}} \left(\frac{|\rho_B - \rho_l|}{\rho_l} \right)^{2/3} \tag{3.38b}$$

It is important, however, to note that in (3.7a)

$$\begin{aligned} Z &= Z_{12} / n_p^f n_B^f \\ &\simeq 5.0 (R_p + R_B)^2 \sqrt{\bar{U}_p^2 + \bar{U}_B^2} \end{aligned} \tag{3.39}$$

is not a true frequency because it has the dimensions of volume/time.

3.2.1.2 Z_{12} With Particle Body Forces

The collision 'frequency' Z, as given by (3.39), has been used in the earlier work of Bloom and Heindel [1997a,b]; this expression, however, does not take into account the (terminal) settling velocity (v_{ps}) of particles or the rise velocity (v_B) of bubbles and is, therefore, not

entirely consistent with the recent expressions for P_c (i.e., (3.13)) and P_{asl} (i.e, (3.17)) which have been derived by Heindel and Bloom ([1998a] and [1998b], respectively). In order to obtain an expression for Z which does take into account both v_{ps} and v_B we return to the general case considered in Section 3.2.1.1 and suppose that the particles in species 1 have a terminal velocity equal to W_{t_1} in the z direction while those of species 2 have terminal velocity W_{t_2}. In an application to particle/bubble interactions

$$W_{t_1} = -|v_{ps}|, \; W_{t_2} = v_B \tag{3.40}$$

In this case the probability distributions for motion in the x and y directions are still governed by expressions of the form (3.27) while for particles of species 1 the probability distribution for velocities in the z-direction must be modified to

$$dP_{1,z} = \frac{1}{\sqrt{2\pi\bar{U}_1^2}} \exp\left[\frac{-(W_1 - W_{t_1})^2}{2\bar{U}_1^2}\right] dW_1 \tag{3.41}$$

with an analogous result for particles of species 2. In lieu of (3.32) and (3.33) we obtain

$$dN_1 = \frac{N_1}{(\sqrt{2\pi\bar{U}_1^2})^3} \exp\left[\frac{-(U_1^2 + V_1^2 + (W_1 - W_{t_1})^2)}{2\bar{U}_1^2}\right] dU_1 dV_1 dW_1 \tag{3.42}$$

and

$$dN_2 = \frac{N_2}{(\sqrt{2\pi\bar{U}_2})^3} \exp\left[\frac{-(U_2^2 + V_2^2 + (W_2 - W_{t_2})^2)}{2\bar{U}_2^2}\right] dU_2 dV_2 dW_2 \tag{3.43}$$

Substituting (3.42), (3.43), and

$$\mathcal{V}_{12} = (U_1 - U_2)^2 + (V_1 - V_2)^2 + [(W_1 - W_{t_1}) - (W_2 - W_{t_2})]^2 \tag{3.44}$$

into (3.35), and then integrating, we obtain in place of (3.36)

$$\begin{aligned} Z_{12} = {} & 2^{3/2}\pi^{1/2} N_1 N_2 d_{12}^2 \sqrt{\bar{U}_1^2 + \bar{U}_2^2} \\ & \times \left\{ \exp\left[-\frac{1}{2} \frac{(W_{t_2} - W_{t_1})^2}{\bar{U}_1^2 + \bar{U}_2^2} \right] \right\} \\ & + N_1 N_2 \pi d_{12}^2 \left\{ \frac{(W_{t_2} - W_{t_1})^2 + \bar{U}_1^2 + \bar{U}_2^2}{W_{t_2} - W_{t_1}} \text{ erf } \left[\frac{W_{t_2} - W_{t_1}}{\sqrt{2(\bar{U}_1^2 + \bar{U}_2^2}} \right] \right\} \end{aligned} \tag{3.45}$$

where the 'error function', erf (x), satisfies

$$\frac{1}{x}\,\text{erf}\,(x) \to 0, \text{ as } x \to 0 \tag{3.46}$$

Because of (3.46), (3.45) converges to the result in (3.36) as $W_{t_2} - W_{t_1} \to 0$.

If we now take into account both the particle settling velocity and the bubble rise velocity in particle/bubble interactions, then from (3.45) we obtain the following modification of (3.39):

$$\begin{aligned} Z = {} & 5.0(R_p + R_B)^2\sqrt{\bar{U}_p^2 + \bar{U}_B^2} \\ & \times \left\{ \exp\left[-\frac{1}{2}\frac{(|v_{ps}| + v_B)^2}{\bar{U}_p^2 + \bar{U}_B^2}\right]\right\} \\ & + \pi(R_p + R_B)^2 \left\{ \frac{(|v_{ps}| + v_B)^2 + \bar{U}_p^2 + \bar{U}_B^2}{|v_{ps}| + v_B}\ \text{erf}\left[\frac{|v_{ps}| + v_B}{\sqrt{2(\bar{U}_p^2 + \bar{U}_B^2)}}\right]\right\} \end{aligned} \tag{3.47}$$

Remarks: In order for the expression (3.47) to be valid, the condition (3.30) must be satisfied. Using (3.11), noting that in our experiments (to be described) $R_{B,\max} \approx 1mm$, $\sigma \approx 35 dynes/cm$, and using water properties

$$\epsilon \approx 1.2 \times 10^4 \frac{cm^2}{s^3} = 1.2\frac{W}{kg} \tag{3.48}$$

The inequality (3.30) is clearly equivalent to

$$\bar{U}^2 < \frac{1}{15}\left(\frac{\epsilon}{\mu_l}\right) d_B^2 \rho_B \tag{3.49}$$

Using (3.48) and the values

$$\left\{ \begin{array}{lcl} \mu_l & = & 1cp \equiv 10^{-2}\ \text{g/cm-sec} \\ d_B & = & 10^{-1}\text{cm} \\ \rho_B & = & 1.13 \times 10^{-3}\ \text{g/cm}^3 \end{array} \right. \tag{3.50}$$

we obtain from (3.49) the restriction that

$$\bar{U} < 0.951\ \text{cm/sec} \tag{3.51}$$

Now,

$$\bar{U} = v_B - \bar{U}_B \tag{3.52}$$

while $\bar{U}_B$ is given by (3.38b). Employing $\rho_l = 1\text{g/cm}^3$ and the values of ϵ, μ_l and d_B in (3.48) and (3.50), we obtain from (3.38b)

$$\bar{U}_B \simeq 20.1 \text{ cm/sec} \tag{3.53}$$

Thus, by virtue of (3.52) and (3.53)

$$\bar{U} \simeq v_B - 20.1 \text{ cm/sec} \tag{3.54}$$

Combining (3.54) with (3.51) we find that (3.30) is satisfied provided

$$v_B \lesssim \bar{U} + 20.1 \text{ cm/sec} \approx 21 \text{ cm/sec} \tag{3.55}$$

Thus a bubble rise velocity, for the laboratory situation considered, of slightly less than 10 cm/sec should suffice to ensure the applicability of the expression (3.47) for Z.

Remarks: We have noted that the derivation of the expression (3.27), for the unidirectional velocity distribution, depends on assumption (3.28) i.e., that the turbulence is in the inertial convection subrange. For the situation under consideration, namely, particle/bubble interactions, $\bar{\lambda} = d_p$ for the first species while $\bar{\lambda} = d_B$ for the second. The Kolmogorov microscale η may be expressed as

$$\eta = \frac{\mu_l^{3/4}}{\rho_l^{3/4}\epsilon^{1/4}} \tag{3.56}$$

and for the values used above, it follows easily from (3.56) that $\eta \simeq 3.02 \times 10^{-3}$cm. For values of d_B and d_p which are given, respectively, by the approximate values of 10^{-1}cm ($R_B = 0.5mm$) and 10^{-2}cm ($R_p = 50\mu m$) the restriction expressed by (3.28) is clearly satisfied.

3.2.2 The Bubble/Particle Detachment Frequency (Z')

The only treatment of the problem of particle/bubble detachment frequency which has been referenced in the literature is that of Mika and Furstenau [1968]; the concept of floc disruption frequency for flocs subject to turbulence in the inertial convection range, governed by (3.28), has been treated by several authors, e.g., Thomas [1964] as well as Parker et al. [1972] and Wågberg and Lindström [1987] and the mechanisms at work in the two different

problems appear to be, fundamentally, the same. As noted in Wågberg and Lindström [1987], "eddies with sizes comparable to the size of fiber flocs are considered to cause disruption of the flocs"; a similar commentary appears in Mika and Furstenau [1968], where vortices of the size of a typical particle/bubble aggregate diameter are thought to be responsible for aggregate destruction. Employing an analysis based on the expression

$$E(k,t) = k_* \epsilon^{2/3} \bar{\lambda}^{5/3} \quad (k = 1/\bar{\lambda}) \tag{3.57}$$

for the energy spectrum, in the inertial convection range (k_* being an empirical turbulence constant) both Thomas [1964] and Parker et al. [1972] derive as the expression for the floc disruption frequency f_λ

$$f_{\bar{\lambda}} = \beta^{1/2} \epsilon^{1/3} \bar{\lambda}^{-2/3} \quad (\beta = 48 k_*) \tag{3.58}$$

In (3.58), $\bar{\lambda}$ is comparable to the eddy sizes of interest, i.e., those of the same order of magnitude as the floc diameter. In using the expression (3.57) for $E(k,t)$, Thomas [1964] attributes a value of $k_* = 0.73$ to Hinze [1959]; using this value of k_* in (3.58) one obtains

$$f_{\bar{\lambda}} = 5.92 \epsilon^{1/3} \bar{\lambda}^{-2/3} \tag{3.59}$$

for the floc disruption frequency in the inertial convection subrange.

Mika and Furstenau [1968] consider a situation in which the turbulence is induced by an impeller blade rotating at high speed; in such a case it has been established that the local energy dissipation has the form

$$\epsilon = K_1 N_I^3 D_I^2 \tag{3.60}$$

where D_I is the impeller diameter, N_I is the rotational speed of the impeller blade, and K_1 is an empirical constant. Employing a turbulence analysis similar to that in the work cited on floc disruption, Mika and Furstenau [1968] find as the expression for the particle/bubble detachment frequency Z'

$$Z' = \sqrt{C_1} K_1^{1/3} N_I D_I^{2/3} (d_p + d_B)^{-2/3} \tag{3.61}$$

where C_1 is a an empirical value whose range is quoted as being $1.61 \leq C_1 \leq 2.33$. Using the expression (3.60) for the local energy dissipation in (3.61) we obtain

$$Z' = \sqrt{C_1}\epsilon^{1/3}(d_p + d_B)^{-2/3} \tag{3.62}$$

which is, formally, of the same structure as the floc disruption frequency $f_{\bar{\lambda}}$ in (3.59); in (3.62) the relevant eddy size $\bar{\lambda}$ is one which is comparable to an aggregate diameter $d_p + d_B$. As ϵ has dimensions L^2t^{-3} it is clear that both $f_{\bar{\lambda}}$, in (3.59), and Z' in (3.62) have dimension t^{-1}, i.e., both expressions represent frequencies. With $C_1 = 2, \epsilon = 1.2m^2/sec^3$, and an aggregate diameter $d_B + d_p \simeq d_B = 10^{-3}m$, one obtains a value of $Z' \approx 150sec^{-1}$.

3.3 The Semi-Batch Process Model

In this section we derive both short-time and low gas holdup solutions for the initial-value problem consisting of (3.24a,b). In (3.24a,b) we recall that $\prime = d/d\tilde{t}$, with $\tilde{t} = t/t^*$ and $t^* = V/Q$, $\epsilon_p = V_B n_B$ is the gas holdup parameter, $E = n_B/n_{po}^f$ where $n_{po}^f = n_p^f(0)$ is the initial concentration of free particles, $\tilde{k}_1$ and $\tilde{k}_2$ are the dimensionless kinetic constants, and α and γ, respectively, are the concentrations of (total) particles and free particles (normalized in each case by n_{po}^f). It is understood that both α and γ in (3.24a,b) are functions of the dimensionless time $\tilde{t}$; thus, the initial conditions associated with these equations have the form

$$\alpha(0) = 1, \ \gamma(0) = 1 \tag{3.63}$$

where we have assumed that $n_p^f(0) = n_p(0)$.

3.3.1 Short-Time Solution

For small $\tilde{t}$ we may expand $\alpha(\tilde{t})$ in a convergent power series in $\tilde{t}$ of the form

$$\alpha(\tilde{t}) = \alpha(0) + \alpha'(0)\tilde{t} + \frac{1}{2}\alpha''(0)\tilde{t}^2 + \frac{1}{6}\alpha'''(0)\tilde{t}^3 + \cdots \tag{3.64}$$

From (3.64) we have $\alpha(0) = 1$ while, by virtue of (3.24a) and (3.65), $\alpha'(0) = 0$. Therefore

$$\alpha(\tilde{t}) = 1 + \frac{1}{2}\alpha''(0)\tilde{t}^2 + \frac{1}{6}\alpha'''(0)\tilde{t}^3 + \cdots \tag{3.65}$$

Differentiating (3.24a) with respect to $\tilde{t}$ and setting, subsequently, $\tilde{t} = 0$, yields

$$\epsilon_p \alpha''(0) = \gamma'(0) \tag{3.66}$$

Setting $\tilde{t} = 0$ in (3.24b) yields

$$\gamma'(0) = -\tilde{k}_1 E \tag{3.67}$$

so that

$$\alpha''(0) = -\tilde{k}_1 E/\epsilon_p \tag{3.68}$$

in which case

$$\alpha(\tilde{t}) = 1 - \frac{\tilde{k}_1 E}{2\epsilon_p}\tilde{t}^2 + \frac{1}{6}\alpha'''(0)\tilde{t}^3 + \cdots \tag{3.69}$$

Differentiating (3.24a) twice, with respect to $\tilde{t}$, yields

$$\alpha'''(0) = \frac{1}{\epsilon_p}\gamma''(0) + \frac{\tilde{k}_1 E}{\epsilon_p^2} \tag{3.70}$$

in which we have also used (3.68). But if we differentiate (3.24b) with respect to $\tilde{t}$, and then set $\tilde{t} = 0$, we find that

$$\gamma''(0) = \tilde{k}_1^2 E^2 + \tilde{k}_1^2 E + \tilde{k}_1 \tilde{k}_2 E \tag{3.71}$$

In obtaining (3.71) we have used $\alpha(0) = \gamma(0) = 1, \alpha'(0) = 0$, and $\gamma'(0) = -\tilde{k}_1 E$. Combining (3.70) with (3.71) yields

$$\alpha'''(0) = \frac{\tilde{k}_1 E}{\epsilon_p^2} + \frac{1}{\epsilon_p}(\tilde{k}_1^2 E^2 + \tilde{k}_1^2 E + \tilde{k}_1 \tilde{k}_2 E) \tag{3.72}$$

The use of (3.72) in (3.69) now yields the solution for small dimensionless time $\tilde{t}$ up to terms of order $\tilde{t}^4$:

$$\boxed{\alpha(\tilde{t}) = 1 - \frac{\tilde{k}_1 E}{2\epsilon_p}\tilde{t}^2 + \left[\frac{\tilde{k}_1 E}{6\epsilon_p^2}(1 + \epsilon_p\{\tilde{k}_1 E + \tilde{k}_1 + \tilde{k}_2\})\right]\tilde{t}^3 + \mathcal{O}(\tilde{t}^4)} \tag{3.73}$$

For sufficiently small $\tilde{t}$ the short-time solution given by the parabolic estimate

$$\boxed{\alpha(\tilde{t}) \simeq 1 - \frac{\tilde{k}_1 E}{2\epsilon_p}\tilde{t}^2} \tag{3.74}$$

which is obtained from (3.73), may suffice outside the low gas holdup (small ϵ_p) regime; however, one must be cautious as (3.74) ignores, to some extent, the effect of particle/bubble destabilization which is governed by $\tilde{k}_2$.

From (3.24a) it follows that

$$\gamma(\tilde{t}) = \epsilon_p \alpha'(\tilde{t}) + \alpha(\tilde{t}) \tag{3.75}$$

From the approximation given by (3.74), and (3.75), we obtain for small $\tilde{t}$:

$$\boxed{\gamma(\tilde{t}) \simeq 1 - \tilde{k}_1 E\tilde{t} - \frac{\tilde{k}_1 E}{2\epsilon_p}\tilde{t}^2} \tag{3.76}$$

We note that (3.74), (3.76) are consistent with $\alpha(0) = \gamma(0) = 1, \alpha'(0) = 0$, and $\gamma'(0) = -\tilde{k}_1 E$. The dimensional form of the short-time solution for $n_p(t)$, up to terms of order t^2, is

$$n_p(t) \simeq n_p(0)\left[1 - \left(\frac{k_1 n_B Q}{2\epsilon_p V}\right)t^2\right] \tag{3.77}$$

while that for $n_p^f(t)$ is

$$n_p^f(t) \simeq n_p(0)\left[1 - k_1 n_B t - \left(\frac{k_1 n_B Q}{2\epsilon_p V}\right)t^2\right] \tag{3.78}$$

3.3.2 Low Gas Holdup Solution

For small gas holdup (ϵ_p) we proceed by looking for solutions of the system (3.24a, b) in the form of perturbation series in the parameter ϵ_p, i.e.,

$$\alpha(\tilde{t}) = \alpha_0(\tilde{t}) + \alpha_1(\tilde{t})\epsilon_p + \alpha_2(\tilde{t})\epsilon_p^2 + \cdots \tag{3.79a}$$

$$\gamma(\tilde{t}) = \gamma_0(\tilde{t}) + \gamma_1(\tilde{t})\epsilon_p + \gamma_2(\tilde{t})\epsilon_p^2 + \cdots \tag{3.79b}$$

We must substitute (3.79a, b) into (3.24a,b), equate like powers of the gas holdup parameter ϵ_p, and determine, successively, the coefficient functions $\alpha_i(\tilde{t}), \gamma_i(\tilde{t}), (i = 0, 1, 2, \cdots)$. Setting $\tilde{t} = 0$ in (3.79a, b) and using $\alpha(0) = \gamma(0) = 1$, we obtain the initial data

$$\begin{array}{l} \alpha_0(0) = 1, \alpha_i(0) = 0, \text{ for } i \geq 1 \\ \gamma_0(0) = 1, \ \gamma_i(0) = 0, \text{ for } i \geq 1 \end{array} \tag{3.80}$$

Next, we insert the expansions (3.79a,b) into (3.24a); equating like powers of ϵ_p we obtain

$$\alpha_0(\tilde{t}) = \gamma_0(\tilde{t}) \tag{3.81}$$

as well as the sequence of first order ODE's

$$\left\{ \begin{array}{rcl} \alpha_0' & = & \gamma_1 - \alpha_1 \\ \alpha_1' & = & \gamma_2 - \alpha_2 \\ & \vdots & \\ \alpha_n' & = & \gamma_{n+1} - \alpha_{n+1} \end{array} \right. \tag{3.82}$$

all of which are subject to the initial data in (3.80). Inserting the expansions (3.79a, b) into (3.24b) yields

$$\begin{array}{c} \gamma_0' + \gamma_1'\epsilon_p + \gamma_2'\epsilon_p^2 + \cdots \\ = -\tilde{k}_1 E(\gamma_0 + \gamma_1\epsilon_p + \gamma_2\epsilon_p^2 + \cdots) \\ +\{\tilde{k}_1(\gamma_0 + \gamma_1\epsilon_p + \gamma_2\epsilon_p^2 + \cdots) + \tilde{k}_2\} \\ \times \left[(\alpha_0 - \gamma_0) + (\alpha_1 - \gamma_1)\epsilon_p + (\alpha_2 - \gamma_2)\epsilon_p^2 + \cdots\right] \end{array} \tag{3.83}$$

Expanding the right-hand side of (3.83), collecting like powers of ϵ_p, and equating like powers of ϵ_p on both sides of (3.83) yields a companion sequence of first order ODE's for (3.82); the

first three equations in this sequence are

$$\gamma_0' = -\tilde{k}_1 E\gamma_0 + (\alpha_0 - \gamma_0)(\tilde{k}_1\gamma_0 + \tilde{k}_2) \tag{3.84a}$$

$$\gamma_1' = -\tilde{k}_1 E\gamma_1 + \tilde{k}_1\gamma_1(\alpha_0 - \gamma_0) + (\tilde{k}_1\gamma_0 + \tilde{k}_2)(\alpha_1 - \gamma_1) \tag{3.84b}$$

$$\begin{aligned}\gamma_2' = &-\tilde{k}_1 E\gamma_2 + \tilde{k}_1\gamma_2(\alpha_0 - \gamma_0) \\ &+\tilde{k}_1(\alpha_1 - \gamma_1) + (\tilde{k}_1\gamma_0 + \tilde{k}_2)(\alpha_2 - \gamma_2)\end{aligned} \tag{3.84c}$$

As $\alpha_0(\tilde{t}) = \gamma_0(\tilde{t})$, i.e. (3.81), equation (3.84a) reduces to

$$\gamma_0' = -\tilde{k}_1 E\gamma_0 \tag{3.85}$$

whose solution subject to $\gamma_0(0) = 1$ is

$$\gamma_0(\tilde{t}) = e^{-\tilde{k}_1 E\tilde{t}} \tag{3.86}$$

Also

$$\alpha_0(\tilde{t}) = e^{-\tilde{k}_1 E\tilde{t}} \tag{3.87}$$

Next, by virtue of (3.86), (3.87), equation (3.84b) reduces to

$$\gamma_1' = -\tilde{k}_1 E\gamma_1 + (\tilde{k}_1\gamma_0 + \tilde{k}_2)(\alpha_1 - \gamma_1) \tag{3.88}$$

However, by the first equation in the set (3.82), and (3.87),

$$\alpha_1 - \gamma_1 = -\alpha_0' = \tilde{k}_1 E e^{-\tilde{k}_1 E\tilde{t}} \tag{3.89}$$

Using (3.89) as well as (3.86), in (3.88), we obtain

$$\gamma_1' + \tilde{k}_1 E\gamma_1 = (\tilde{k}_1 e^{-\tilde{k}_1 E\tilde{t}} + \tilde{k}_2)\tilde{k}_1 E e^{-\tilde{k}_1 E\tilde{t}} \tag{3.90}$$

The solution of (3.90), subject to the initial condition $\gamma_1(0) = 0$, is easily seen to be

$$\gamma_1(\tilde{t}) = \tilde{k}_1(e^{-\tilde{k}_1 E\tilde{t}} - e^{-2\tilde{k}_1 E\tilde{t}}) + \tilde{k}_1\tilde{k}_2\tilde{t}e^{-\tilde{k}_1 E\tilde{t}} \tag{3.91}$$

From the first equation in the set (3.82), as well as (3.87) and (3.91), one easily finds that

$$\alpha_1(\tilde{t}) = \tilde{k}_1(1+E)e^{-\tilde{k}_1 E\tilde{t}} - \tilde{k}_1 e^{-2\tilde{k}_1 E\tilde{t}} + \tilde{k}_1\tilde{k}_2 E\tilde{t}e^{-\tilde{k}_1 E\tilde{t}} \tag{3.92}$$

Finally, using (3.84c), (3.86), (3.87), (3.91), and (3.92) we have

$$\begin{aligned}\gamma_2' + \tilde{k}_1 E\gamma_2 = \tilde{k}_1^2 E e^{-\tilde{k}_1 E\tilde{t}}\left\{\tilde{k}_1(e^{-\tilde{k}_1 E\tilde{t}} - e^{-2\tilde{k}_1 E\tilde{t}}) + \tilde{k}_1\tilde{k}_2\tilde{t}e^{-\tilde{k}_1 E\tilde{t}}\right\} \\ +(\tilde{k}_1 e^{-\tilde{k}_1 E\tilde{t}} + \tilde{k}_2)(\alpha_2 - \gamma_2)\end{aligned} \tag{3.93}$$

However, by virtue of the second equation in the set (3.82), and (3.92),

$$\begin{aligned}\alpha_2 - \gamma_2 = \tilde{k}_1^2 E(1+E)e^{-\tilde{k}_1 E\tilde{t}} - 2\tilde{k}_1^2 E e^{-2\tilde{k}_1 E\tilde{t}} \\ -\tilde{k}_1\tilde{k}_2 E e^{-\tilde{k}_1 E\tilde{t}} + \tilde{k}_1^2\tilde{k}_2 E^2\tilde{t}e^{-\tilde{k}_1 E\tilde{t}}\end{aligned} \tag{3.94}$$

Substituting (3.94) into (3.93), and collecting terms, we arrive at the equation

$$\gamma_2' + \tilde{k}_1 E\gamma_2 = \phi(\tilde{k}_1, \tilde{k}_2, E; \tilde{t}) \tag{3.95}$$

where

$$\begin{aligned}\phi \equiv \tilde{k}_1\tilde{k}_2 E(\tilde{k}_1(1+E) - \tilde{k}_2)e^{-\tilde{k}_1 E\tilde{t}} \\ +\tilde{k}_1^2 E(\tilde{k}_1 + \tilde{k}_1(1+E) - \tilde{k}_2)e^{-2\tilde{k}_1 E\tilde{t}} \\ -\tilde{k}_1^2 E(1+2\tilde{k}_1)e^{-3\tilde{k}_1 E\tilde{t}} \\ +\tilde{k}_1^2\tilde{k}_2^2 E\tilde{t}e^{-\tilde{k}_1 E\tilde{t}} + \tilde{k}_1^3\tilde{k}_2 E(1+E)\tilde{t}e^{-2\tilde{k}_1 E\tilde{t}}\end{aligned} \tag{3.96}$$

Solving (3.95), subject to $\gamma_2(0) = 0$, then produces for γ_2 the following result:

$$\gamma_2(\tilde{t}) = (\bar{a} + \bar{b}\tilde{t} + \bar{c}\tilde{t}^2)e^{-\tilde{k}_1 E\tilde{t}} + \bar{d}e^{-2\tilde{k}_1 E\tilde{t}} + \bar{e}e^{-3\tilde{k}_1 E\tilde{t}} \tag{3.97}$$

where the constants $\bar{a}, \bar{b}, \bar{c}, \bar{d}$, and $\bar{e}$ are defined by

$$\bar{a} = \tilde{k}_1(\tilde{k}_1 - \tilde{k}_2) + \tilde{k}_2(1+E)\left(1 + \frac{1}{\tilde{k}_1 E}\right) - \frac{1}{2}\tilde{k}_1(1+2\tilde{k}_1) \tag{3.98a}$$

$$\bar{b} = \tilde{k}_1\tilde{k}_2 E(\tilde{k}_1(1+E) - \tilde{k}_2) \tag{3.98b}$$

$$\bar{c} = \frac{1}{2}\tilde{k}_1^2\tilde{k}_2^2 E \tag{3.98c}$$

$$\bar{d} = \tilde{k}_1(\tilde{k}_1 - \tilde{k}_2) + \tilde{k}_2(1+E) + \tilde{k}_1^2\tilde{k}_2(1+E)\left(1 + \frac{1}{\tilde{k}_1 E}\right) \tag{3.98d}$$

$$\bar{e} = \frac{1}{2}\tilde{k}_1(1+2\tilde{k}_1) \tag{3.98e}$$

From the second equation in the set (3.82) we have $\alpha_2 = \gamma_2 - \alpha_1'$; therefore, employing (3.92) in conjunction with (3.97) we find that

$$\alpha_2(\tilde{t}) = [\hat{a} + \hat{b}\tilde{t} + \hat{c}\tilde{t}^2]e^{-\tilde{k}_1 E\tilde{t}} + \hat{d}e^{-2\tilde{k}_1 E\tilde{t}} + \hat{e}e^{-3\tilde{k}_1 E\tilde{t}} \tag{3.99}$$

with

$$\hat{a} = \bar{a} + (\tilde{k}_1^2 E(1+E) - \tilde{k}_1\tilde{k}_2 E) \tag{3.100a}$$

$$\hat{b} = \bar{b} + \tilde{k}_1^2\tilde{k}_2 E \tag{3.100b}$$

$$\hat{c} = \bar{c} \tag{3.100c}$$

$$\hat{d} = \bar{d} - 2\tilde{k}_1^2 E \tag{3.100d}$$

$$\hat{e} = \bar{e} \tag{3.100e}$$

Inserting the results for $\gamma_0(\tilde{t})$, $\gamma_1(\tilde{t})$, and $\gamma_2(\tilde{t})$, i.e., (3.86), (3.91), and (3.97), into (3.79b) now yields, up to terms of order ϵ_p^3,

$$\boxed{\begin{aligned}\gamma(\tilde{t}) = e^{-\tilde{k}_1 E\tilde{t}} + [\tilde{k}_1(e^{-\tilde{k}_1 E\tilde{t}} - e^{-2\tilde{k}_1 E\tilde{t}}) + \tilde{k}_1\tilde{k}_2 E\tilde{t}e^{-\tilde{k}_1 E\tilde{t}}]\epsilon_p \\ +[(\bar{a} + \bar{b}\tilde{t} + \bar{c}\tilde{t}^2)e^{-\tilde{k}_1 E\tilde{t}} + \bar{d}e^{-2\tilde{k}_1 E\tilde{t}} + \bar{e}e^{-3\tilde{k}_1 E\tilde{t}}]\epsilon_p^2 + \mathcal{O}(\epsilon_p^3)\end{aligned}} \tag{3.101}$$

Similarly, inserting the results for $\alpha_0(\tilde{t})$, $\alpha_1(\tilde{t})$ and $\alpha_2(\tilde{t})$, i.e., (3.87), (3.92), (3.99) into the perturbation expansion (3.79a) yields, up to terms of order ϵ_p^3,

$$\boxed{\begin{aligned}\alpha(\tilde{t}) = e^{-\tilde{k}_1 E\tilde{t}} + [\tilde{k}_1(1+E)e^{-\tilde{k}_1 E\tilde{t}} - \tilde{k}_1 e^{-2\tilde{k}_1 E\tilde{t}} + \tilde{k}_1\tilde{k}_2 E\tilde{t}e^{-\tilde{k}_1 E\tilde{t}}]\epsilon_p \\ +[(\hat{a} + \hat{b}\tilde{t} + \hat{c}\tilde{t}^2)e^{-\tilde{k}_1 E\tilde{t}} + \hat{d}e^{-2\tilde{k}_1 E\tilde{t}} + \hat{e}e^{-3\tilde{k}_1 E\tilde{t}}]\epsilon_p^2 + \mathcal{O}(\epsilon_p^3)\end{aligned}} \tag{3.102}$$

Dimensional expressions for $n_p^f(t)$ and $n_p(t)$, respectively, may be easily produced by using (3.101), (3.102) and the definitions of $\tilde{k}_1, \tilde{k}_2$, E, and $\tilde{E}$ in conjunction with (3.98a-e) and (3.100a-e).

3.4 Model Summary

In this section we will briefly summarize the model equations and their approximate solutions in the short-time and low gas holdup regimes. The semi-batch process model equations are (3.24a,b), i.e.,

$$\epsilon_p\alpha' = -(\alpha - \gamma) \tag{3.24a}$$

$$\gamma' = -\tilde{k}_1 E\gamma + \tilde{k}_1\gamma(\alpha - \gamma) + \tilde{k}_2(\alpha - \gamma) \tag{3.24b}$$

In (3.24a,b), $' = \dfrac{d}{d\tilde{t}}$, i.e., differentiation with respect to the dimensionless time $\tilde{t} = t/t^*$ where $t^* = V/Q$. The normalized total particle and free particle concentrations enter (3.24a,b) as

$$\alpha = n_p/n_{po}^f \text{ and } \gamma = n_p^f/n_{po}^f,$$

respectively, where $n_{po}^f = n_p^f(0) \equiv n_p(0)$. The dimensionless attachment and detachment rates $\tilde{k}_1$ and $\tilde{k}_2$, respectively, are given by

$$\tilde{k}_1 = k_1 t^* n_{po}^f \text{ and } \tilde{k}_2 = k_2 t^*$$

where, by (3.7a,b),

$$k_1 = Z P_c P_{asl} P_{tpc} P_{stab} \tag{3.7a}$$

$$k_2 = Z' P_{destab} = Z'(1 - P_{stab}) \tag{3.7b}$$

In (3.7a,b) $P_{tpc} \simeq 1$, P_{stab} is given by (3.8) and (3.9), P_c by (3.13), P_{asl} by (3.17), and the collision 'frequencies' Z and Z' by (3.47) and (3.62), respectively. Finally, the parameters ϵ_p (gas holdup per unit volume) and E (the relative bubble concentration with respect to the initial concentration of ink particles) in (3.24a,b) are defined by

$$\epsilon_p = V_B n_B \text{ and } E = n_B/n_{po}^f,$$

respectively, with n_B the constant concentration of air bubbles per unit volume in the column, as given by (3.4), and V_B the volume of a single bubble. The system (3.24a,b) is subject to the initial conditions

$$\alpha(0) = 1, \;\; \gamma(0) = 1$$

For small $\tilde{t}$ (short-time) we have found that, up to terms of order $\mathcal{O}(t^4)$, (3.73) holds, i.e.,

$$\alpha(\tilde{t}) \simeq 1 - \frac{\tilde{k}_1 E}{2\epsilon_p}\tilde{t}^2 + \left[\frac{\tilde{k}_1 E}{6\epsilon_p^2}(1 + \epsilon_p\{\tilde{k}_1 E + \tilde{k}_1 + \tilde{k}_2\})\right]\tilde{t}^3$$

and, then, by virtue of (3.24a)

$$\gamma(\tilde{t}) = \epsilon_p \alpha'(\tilde{t}) + \alpha(\tilde{t})$$

For very small $\tilde{t}$, (3.73) may be replaced by the parabolic estimate (3.74), i.e.,

$$\alpha(\tilde{t}) \simeq 1 - \frac{\tilde{k}_1 E}{2\epsilon_p}\tilde{t}^2$$

in which case (3.75) leads to (3.76), i.e.,

$$\gamma(\tilde{t}) \simeq 1 - \tilde{k}_1 E\tilde{t} - \frac{\tilde{k}_1 E}{2\epsilon_p}\tilde{t}^2$$

Other estimates are also available as a consequence of (3.73), (3.75), e.g., if

$$\epsilon_p(\tilde{k}_1[1+E] + \tilde{k}_2) << 1$$

then from (3.73) we have

$$\alpha(\tilde{E}) \simeq 1 - \frac{\tilde{k}_1 E}{2\epsilon_p}\tilde{t}^2 + \frac{\tilde{k}_1 E}{6\epsilon_p^2}\tilde{t}^3 \tag{3.103}$$

in which case (3.75) produces

$$\gamma(\tilde{t}) \simeq 1 - \tilde{k}_1 E\tilde{t} + \frac{\tilde{k}_1 E}{6\epsilon_p^2}\tilde{t}^3 \tag{3.104}$$

From (3.74), (3.76) we have

$$\alpha(\tilde{t}) - \gamma(\tilde{t}) = \tilde{k}_1 E\tilde{t} \equiv k_1 n_B t > 0 \tag{3.105}$$

for all sufficiently small $t > 0$, while from (3.103), (3.104)

$$\alpha(\tilde{t}) - \gamma(\tilde{t}) = \tilde{k}_1 E\tilde{t} - \frac{\tilde{k}_1 E}{2\epsilon_p}\tilde{t}^2 = \tilde{k}_1 E\tilde{t}\left(1 - \frac{1}{2\epsilon_p}\tilde{t}\right) > 0$$

only for $\tilde{t} < 2\epsilon_p$, i.e., for

$$t < \frac{2V}{Q}(n_B V_B) \tag{3.106}$$

The inequality (3.106) serves to make precise the meaning of 'short-time' with respect to the application of the estimates (3.103), (3.104); on the other hand, the somewhat cruder estimates (3.74), (3.76) are applicable provided that (3.73) may be replaced by (3.74), i.e., provided that $\tilde{t} << 1$, or

$$t << \frac{V}{Q} \tag{3.107}$$

For the case of low gas holdup (small ϵ_p) we have obtained the following results which are based on substituting the perturbation series (3.79a,b) into (3.24a,b), imposing the initial conditions $\alpha(0) = \gamma(0) = 1$, and equating like powers of ϵ_p: Define the two families of constants

$$(i) \quad \begin{cases} \bar{a} = \tilde{k}_1(\tilde{k}_1 - \tilde{k}_2) + \tilde{k}_2(1+E)\left(1 + \dfrac{1}{\tilde{k}_1 E}\right) - \dfrac{1}{2}\tilde{k}_1(1+2\tilde{k}_1) \\ \bar{b} = \tilde{k}_1\tilde{k}_2 E(\tilde{k}_1(1+E) - \tilde{k}_2) \\ \bar{c} = \dfrac{1}{2}\tilde{k}_1^2\tilde{k}_2^2 E \\ \bar{d} = \tilde{k}_1(\tilde{k}_1 - \tilde{k}_2) + \tilde{k}_2(1+E) + \tilde{k}_1^2\tilde{k}_2^2(1+E)\left(1 + \dfrac{1}{\tilde{k}_1 E}\right) \\ \bar{e} = \dfrac{1}{2}\tilde{k}_1(1+2\tilde{k}_1) \end{cases}$$

and

$$(ii) \quad \begin{cases} \hat{a} = \bar{a} + (\tilde{k}_1^2 E(1+E) - \tilde{k}_1\tilde{k}_2 E) \\ \hat{b} = \bar{b} + \tilde{k}_1^2\tilde{k}_2 E \\ \hat{c} = \bar{c} \\ \hat{d} = \bar{d} - 2\tilde{k}_1^2 E \\ \hat{e} = \bar{e} \end{cases}$$

then up to terms of order ϵ_p^3, for ϵ_p small:

$$\begin{aligned} \alpha(\tilde{t}) \simeq e^{-\tilde{k}_1 E\tilde{t}} &+ \left[\tilde{k}_1(1+E)e^{-\tilde{k}_1 E\tilde{t}} - \tilde{k}_1 e^{-2\tilde{k}_1 E\tilde{t}} + \tilde{k}_1\tilde{k}_2 E\tilde{t}e^{-\tilde{k}_1 E\tilde{t}}\right]\epsilon_p \\ &+ \left[(\hat{a} + \hat{b}\tilde{t} + \hat{c}\tilde{t}^2)e^{-\tilde{k}_1 E\tilde{t}} + \hat{d}e^{-2\tilde{k}_1 E\tilde{t}} + \hat{e}e^{-3\tilde{k}_1 E\tilde{t}}\right]\epsilon_p^2 \end{aligned} \tag{3.108}$$

and

$$\begin{aligned} \gamma(\tilde{t}) \simeq e^{-\tilde{k}_1 E\tilde{t}} &+ \left[\tilde{k}_1(\bar{e}^{\tilde{k}_1 E\tilde{t}} - e^{-2\tilde{k}_1 E\tilde{t}}) + \tilde{k}_1\tilde{k}_2 E\tilde{t}e^{-\tilde{k}_1 E\tilde{t}}\right]\epsilon_p \\ &+ \left[(\bar{a} + \bar{b}\tilde{t} + \bar{c}\tilde{t}^2)e^{-\tilde{k}_1 E\tilde{t}} + \bar{d}e^{-2\tilde{k}_1 E\tilde{t}} + \bar{e}e^{-3\tilde{k}_1 E\tilde{t}}\right]\epsilon_p^2 \end{aligned} \tag{3.109}$$

4 EXPERIMENTAL PROCEDURES

Flotation experiments were completed to determine particle removal efficiencies for various size ranges of toner particles. This section summarizes the procedures used in these experiments. The model flotation cell will first be described. Then stock preparation procedures and experimental conditions will be outlined. Finally, the data analysis procedures will be reviewed.

4.1 Model Flotation Cell

A schematic of the model flotation cell is shown in Fig. 1. It consisted of a 6.4 cm diameter clear acrylic cylinder that was 68.6 cm long. One end of the cylinder was attached to a conical section, where the cone apex contained a sintered stainless steel sparger with 40 μm openings. The sparger location also acted as a sampling port when the experiment was completed. The opposite end of the cylinder was open to allow for foam removal. The flotation column was vertically mounted in a test stand such that the sparger was located at the column base. A low-speed agitator (i.e., mixer) was used to prevent fiber flocculation and help keep the stock mixed.

4.2 Stock Preparation

The stock used in these flotation trials consisted of fused toner particles that were added to unprinted copy paper and then repulped.

4.2.1 Toner Particle Generation

To eliminate the complication of "hairy" toner particles [Johnson and Thompson, 1995; Pan et al., 1995; Vidotti et al., 1995a, b; Thompson, 1997], our experiments were completed with toner particles that were fused prior to pulp addition. Following the procedures of Vidotti et al. [1997], images were printed on cellophane using an HP-6P laser printer with a LaserLife Toner Cartridge (LL C3903A). The images were composed of twelve black rectangles, each with an area of 11.2 cm^2. Therefore, each sheet had approximately 22% printed area. The image regions were then soaked in DI water and the fused toner separated from the cellophane. This procedure was completed multiple times to generate a sufficient amount of fused toner particles for each flotation trial.

4.2.2 Fiber/Toner Mixture

A number of unprinted copy paper sheets (i.e., 20) were shredded and soaked in DI water following TAPPI Method T 205 om-88. Fused toner particles from nine (9) cellophane

sheets where then added to the soaked copy paper and disintegrated following standard TAPPI procedures. This disintegration procedure ensured no "hairy" toner particles were present in the suspension, and that the true toner particle size effects could be addressed during the flotation experiments. This process also resulted in a wide distribution of toner particle sizes. Figure 2 displays the particle size distribution from three separate feed trials, showing the uniformity in the particle size from trial to trial. These data will be discussed in detail below.

4.3 Experimental Conditions

Flotation trials were performed for a given time period ranging from 2 to 60 minutes. Each trial consisted of a known volume of stock with the added toner particles. Initial trials were completed with 1 L of 1% stock. Triton X-100, henceforth identified as TX-100, was used as the foaming agent in all trials, and was added at a rate of 200 mg of TX-100 per liter of 1% stock.

During the flotation trial, zero purity air (Air Products) was injected through the sparger at a constant rate of 1 L/min . Foam was generated throughout the flotation period and was removed at the column top. After a specified flotation period, the sparger was removed from the column base and a 500 ml sample of the remaining stock was collected. This sample represented the accepts from the flotation trial and was collected from the column bottom to eliminate the possibility of collecting some foam with the accepts. Therefore, particles transported to the foam were assumed to be removed from the system. The remaining stock from the trial was discarded.

This flotation procedure was repeated for each specified flotation time, using a new 1 L stock sample from a feed bucket for each trial.

4.4 Data Analysis

4.4.1 Surface Tension Measurements

The surface tension of the accept filtrate from selected trials was measured using a Dynamic Contact Angle Analyzer. Since the experiment was performed in a batch process, the accept stream surface tension varied with flotation time. This result was due to the air bubbles transporting some of the surfactant to the foam layer, where it was removed with the foam. Figure 3 displays how surface tension varied with flotation time for these experiments. As expected, the lowest surface tension corresponds to the initial conditions. The surface tension then increases with increasing flotation time toward the value associated with DI water. Since data for only the first 10 minutes of flotation was used in the model validation, a constant surface tension value was estimated for use in the model predictions. For these calculations, the surface tension was fixed at $\sigma \approx 35$ dynes/cm. The effect of surface tension variations will be addressed in Section 5.4.1.

4.4.2 Handsheet Preparation

Handsheets from the feed and accepts of each trial were prepared following standard TAPPI handsheet making procedures with two modifications. First, very thin handsheets were made (15-20 g/m^2) to reduce the likelihood that the handsheets were two-sided. Second, the handsheets were formed in a British Handsheet Mold, but filter paper (VWR Brand #415) was placed on the screen before the handsheet was formed. This prevented the loss of any toner particles that could pass through the screen. Note that when making these handsheets, dilution water was added from the top of the handsheet mold to prevent damage to the filter paper.

4.4.3 Image Analysis

Image analysis was performed on three handsheets from each flotation trial to obtain a representative sample of the particle removal efficiencies. Five random image fields were scanned, with a 1500 dpi resolution, from each handsheet. Each field represented approxi-

mately 5.4 cm^2. Optimas 5.2 image analysis software was used to determine the particle size of all toner particles found in the random areas. The equivalent diameter, defined as the circular diameter whose area is equal to that of the particle, was then determined for each particle. Particles with an equivalent diameter larger than 50 μm could be identified with this procedure. (A new image analysis system has recently been purchased that will allow for improved analysis at smaller particle resolutions.)

5 RESULTS

This section presents the experimental particle removal efficiencies obtained in the flotation trials, compares these efficiencies with predicted values, and provides possible reasons for the discrepancies between the experimental data and the theoretical model. This section concludes with a limited parametric model study to show the model sensitivity to selected variables.

5.1 Experimental Results

Figure 4 presents the particle concentrations for the flotation trials identified as Trial 1. This represents flotation trials for various flotation times using the same feed stock. Trials 2 and 3, discussed below, represent similar flotation trials, but from different feed stock. The effective particle diameter is classified in 50 μm wide bins, beginning at 50 μm. From the image analysis and the exact handsheet basis weight, the particle concentration is determined as the number of particles per gram o.d. fiber. This assumes that the handsheet formation is uniform and the ink particle mass is negligible. Both of these assumptions are reasonable. The feed sample (solid symbols) provides a high (and fairly uniform) particle concentration over a wide range of effective particle diameters. The concentration begins to decrease after approximately 300 μm. There is also a high particle concentration for particles larger than 400 μm, but these particles include a wide size distribution (i.e., approximately 400-1000 μm).

Performing flotation for various time periods on this feed stock results in a decrease in particle concentration with increasing flotation time. There is a significant decrease in particle concentration between the 10 and 20 minute flotation periods. There is also a negligible difference from one particle size range to another as flotation time increases. After 30 minutes of flotation, nearly all particles are removed, and after 60 minutes of flotation, only a few particles are visible in the entire accept sample. For this reason, the 60 minute flotation data have been removed from Fig. 4 and all subsequent figures.

The experimental particle removal efficiency can be defined by

$$\text{Eff(t)} = 1 - \frac{\text{Accept Particle Concentration}}{\text{Feed Particle Concentration}} \times 100\% \tag{5.1}$$

This value is shown in Fig. 5 for the Trial 1 data. As expected, the removal efficiency is initially low, but increases with increasing flotation time. Figure 5 also shows that particles in the 50-100 μm size range are initially removed more effectively than very large ($> 400\mu$m) particles. However, after 20 minutes of flotation, all particles have a high removal efficiency. After 30 minutes of flotation, the removal efficiency for all particle size ranges approached 100%. This was also visually confirmed by viewing the individual handsheets for the 30 minute trial - they only had a few particles on them.

Two additional flotation trials were completed, and the particle concentrations and removal efficiencies for these trials are shown in Figs. 6-9. As shown, similar trends are observed to those of Trial 1 and good repeatability between the three trials was obtained. This is also shown in Appendix Table A.1, where the flotation efficiency for each condition is summarized.

The average particle removal efficiency, as a function of flotation time, from all three trials for each particle size range is shown in Fig. 10. As expected, the removal efficiency increases with increasing flotation time. For the conditions of this study, there also appears to be only small variations between each particle size range. It is hypothesized that this result is due to the low mixing intensity (i.e., turbulence) in the flotation cell, and the ramifications of

this will be discussed in Section 5.3.

5.2 Comparisons to Model Predictions

Comparisons between our flotation model and this initial data have been made. In these comparisons, $\gamma(t)$ is defined as

$$\gamma(t) = \frac{n_p^f(t)}{n_{po}^f} = \frac{\text{Accept Particle Concentration}}{\text{Feed Particle Concentration}} \tag{5.2}$$

The gas holdup in the various experiments was recorded to be approximately 2.2%. Therefore, $\epsilon_p = 0.022$ in (3.101) and, as a first approximation, second-order and higher terms involving ϵ_p will be neglected in (3.101). Hence, on a dimensional basis, (3.101) reduces to

$$\gamma(t) \approx e^{-k_1 n_B t} + \left[k_1 \left(\frac{V}{Q}\right) n_{po}^f (e^{-k_1 n_B t} - e^{-2k_1 n_B t}) + \left(\frac{V}{Q}\right) n_B k_1 k_2 t e^{-k_1 n_B t}\right] \epsilon_p \tag{5.3}$$

The experimental data, as a function of time, for each particle size range is then fit to (5.3) to determine k_1 and k_2. Only the first 10 minutes of flotation were used in these comparisons because $\gamma(t)$ approached zero for the larger flotation times (i.e., experimental removal efficiencies approaching 1). More data will be collected for $t \leq 10$ minutes in subsequent flotation trials.

Based on bubble size measurements completed in a TX-100 saturated solution, the bubble radius (R_B) was between 0.4 and 0.6 mm, and the maximum bubble radius was approximately 1.0 mm. This information was used in conjunction with the gas holdup (ϵ_p) to estimate the number of bubbles per unit volume (n_B). The initial number of free particles in a given size range (n_{po}^f) was determined from image analysis of the feed stream.

A sample plot of $\gamma(t)$ is shown in Fig. 11 for the particle size range of 100-150 μm. The midpoint particle radius ($R_p = 62.5\mu m$) is used to characterize this particle size range. Flotation results for up to 10 minutes of flotation are included in the figure. The experimental data follow a decaying exponential curve. The "best fit" to (5.3) has been determined to be

with $k_1 = 3.4 \times 10^{-8}$ and $k_2 = -4.8 \times 10^{-4}$ ($R^2 = 0.87$). This curve is also included in Fig. 11. The experimentally determined k_1 and k_2 values for other particle size ranges are shown in Table 1.

This table highlights two unexpected results: (1) the experimentally determined k_1 values are very similar for all particle size ranges; and (2) the "best fit" to the data includes negative k_2 values which physically should be a positive number. It is hypothesized that these results are due to the experimental facility creating only minor turbulence (mixing) in the flotation cell. Therefore, if a bubble/particle is formed, it is unlikely that turbulence would destabilize the aggregate. This will be further discussed below. Low turbulent mixing would also cause k_2 (the kinetic constant describing bubble/particle aggregate destruction) to have only a minor influence on $\gamma(t)$ in (5.3). The negative k_2 was determined simply from a "best fit" curve fitting technique.

To show that k_2 does indeed have only a minor influence on the results in this these experiments, k_1 was also determined through a "best fit" curve fit while k_2 was fixed at one of two values. The first corresponds to $k_2 = 0$ (no destabilization of the bubble/particle aggregate), and the second corresponds to k_2 set to the theoretically determined value (3.7b). These results are also included in Table 1. For a fixed R_p, k_2 has a very minor effect on the value determined for k_1 when the magnitude of k_2 is small. Therefore, for the resulting experimental conditions of this study, k_2 plays an insignificant roll. It is expected that this is not the case in actual flotation cells, and the experimental conditions in upcoming laboratory flotation trials will be modified to correct for this deficiency (see Sections 5.3 and 7).

To determine the predicted k_1 and k_2 values, based on our model, additional assumptions were made. These include: (1) the particle size was fixed at the midpoint particle radius for the size range considered for each condition; (2) the bubble size was fixed at a bubble radius of $R_B \approx 0.5$ mm, the midpoint of the bubble size measurements; (3) the liquid surface tension was fixed at $\sigma \approx 35$ dynes/cm, even though it varied with flotation time; (4) the turbulent energy density was determined from (3.11) using the appropriate values for surface

tension ($\sigma \approx 35$ dynes/cm), maximum bubble radius ($R_{B,\max} \approx 1$ mm), and fluid density ($\rho_1 \approx 1$ g/cm^3); (5) the surface mobility coefficient was specified as $C_B = 1$, corresponding to an idealized rigid bubble surface; and (6) the ratio of initial-to-critical film thickness was taken to be $h_0/h_{crit} = 3$.

The theoretical value of $\gamma(t)$ for $R_p = 62.5\mu$m is also shown in Fig. 11 and is near 1 for the majority of the shown flotation time (i.e., prediction (1)). The predicted k_1 and k_2 values for the theoretical $\gamma(t)$ for the conditions in Fig. 11 are 2.0×10^{-9} and 1.4×10^{-1}, respectively. These values do not match the experimental conditions very well. Table 2 summarizes the theoretical k_1 and k_2 values for the same particle size ranges shown in Table 1. In all cases, the theoretical k_1 is approximately 5 to 50 times smaller than the experimentally determined value. For the experimental conditions used here, k_2 had a negligible influence on the results so it is inappropriate to compare the experimental and theoretical k_2 values. Potential reasons for the discrepancies in k_1 and k_2 will be detailed in the next section. However, it is instructive to show that slight variations in two parameters, C_B and h_0/h_{crit}, which have been estimated from the mineral flotation literature but are unknown for our system, can have a significant effect on the predictions. For example, prediction (2) in Fig. 11 maintains all the same values as prediction (1), except $C_B = 2$ and $h_0/h_{crit} = 2$. This produces a predicted k_1 (k_2 does not change) of 2.3×10^{-8}, which is much closer to the experimental values. Although C_B and h_0/h_{crit} were varied only slightly, they have a large impact on the predicted k_1 values. These variations will be highlighted in Section 5.4.

Combining (5.1) and (5.2), flotation efficiency can be described by

$$Eff(t) = 1 - \gamma(t) \tag{5.4}$$

The flotation efficiency for the conditions shown in Fig. 11 is presented in Fig. 12. The under prediction of the theoretical flotation efficiency is the primary result of the under prediction of k_1. However, slight changes to C_B and h_0/h_{crit} greatly improves these predictions.

5.3 Discrepancy Explanation

This section presents potential reasons for the wide discrepancies between the experimental and theoretical kinetic constants k_1 and k_2. Possible experimental and theoretical problems are outlined and potential solutions to these problems are presented.

5.3.1 Experimental

After obtaining and analyzing all of the experimental data, it has been determined that the model flotation cell used in this study had one serious flaw. That is, very little turbulence was produced in the flotation cell. This allowed all bubble/particle aggregates that formed to remain stable as they rose to the froth layer (i.e., $P_{stab} \approx 1$), Therefore, as shown in Table 1, k_2 had a negligible effect on the overall results. This would not be true in actual flotation cells because severe mixing is typically introduced [Heindel, 1999].

To correct this deficiency, future laboratory flotation trials will use a Wemco flotation cell. This type of flotation cell also operates as a batch process. However, it is a *standard* laboratory flotation cell with considerable mixing. Figure 13 is a schematic representation of this cell. It consists of a 3.5 L plastic tank, an impeller and perforated stabilizer, and a hollow stainless steel shaft. It is equipped with a variable speed rotor (300-1900 RPM) and a gas inlet valve. With the gas inlet open to the atmosphere, the aeration rate is a function of the impeller speed. However, if the gas inlet is connected to pressurized air, the air flow can be metered into the cell. Therefore, the aeration rate can be controlled independently from the impeller speed.

5.3.2 Theoretical

Recall that two (major) assumptions were included in the flotation model [Heindel and Bloom, 1995]: (1) a bubble can pick up at most one particle and carry it to the surface of the flotation cell, and (2) all particles are spherical. These assumptions were made in order to solve the initial model equations. However, bubbles in actual flotation cells will carry more

than one particle to the surface, and particles, particularly toner particles, are non-spherical. We believe the first assumption is the most restrictive. If more than one particle is allowed to attach to a bubble, which is more realistic, k_1 will be larger and the predicted efficiency will also be higher. We are currently in the process of removing this severe restriction to our model equations, and it is expected that the predictions will be much closer to the experimental values.

In addition to this severe restriction, other factors may also influence the theoretical predictions. For example, certain parameters must be know to determine the various micro-process probabilities. The effect of variations in three of these parameters on the theoretical kinetic constants are presented in Section 5.4. Additionally, some of the needed information is determined from the mineral flotation literature because the two flotation processes are commonly assumed to be similar (see Heindel [1999] and the citations therein). However, their direct applicability to flotation deinking has yet to be verified.

5.4 Limited Parametric Studies

Various parameters must be known before the theoretical k_1 and k_2 values can be determined. This section presents limited parametric studies for three of these parameters: the surface tension (σ), the surface mobility coefficient (C_B) , and the ratio of initial-to-critical film thickness (h_0/h_{crit}). These calculations were completed for the conditions outlined in Table 3. All parameters are fixed at these conditions except for the one that was varied.

5.4.1 Effect of Surface Tension

The surface tension of a flotation deinking liquor can easily be measured and may be assumed to be approximately constant in a continuous flotation process. However, in a batch flotation process like the one carried out in the laboratory, surface tension does not remain constant because some of the surfactant that is used as a frothing agent is removed with the foam (e.g., Fig. 3). However, in the model, it is assumed to be independent of time. Therefore, it is of interest to determine the impact surface tension variations have on both k_1

and k_2. A minimum surface tension in our experiments is on the order of 30 dynes/cm and a maximum would correspond to DI water (~72 dynes/cm). Therefore, the surface tension could vary between ~30 and ~70 dynes/cm, but as shown in Fig. 3, in most trials it will range between 30 and 40 dynes/cm.

Figure 14 shows how k_1 and k_2 vary as the surface tension in increased from 20 to 70 dynes/cm. Over this wide range of surface tensions, both k_1 and k_2 increase by approximately a factor of 2. In the surface tension range encountered in most of the experiments (30-40 dynes/cm), k_1 increases by a factor of ~1.30 and k_2 increases by a factor of ~1.15. This variation is not considered to be a major influence on the theoretical results.

5.4.2 Effect of the Surface Mobility Coefficient

The bubble surface mobility coefficient, C_B, characterizes the degree of immobilization of the bubble surface due to the influence of the adsorption layer of surfactant on the bubble surface. It will influence k_1 through P_{asl} and has been shown to vary between 1 and 4, depending on the surfactant concentration. For pure water $C_B = 4$, and for a completely rigid surface $C_B = 1$. Figure 15 shows that k_1 increases by over an order of magnitude as C_B increases from 1 to 4. However, since an air bubble in a deinking system is more likely to act as a rigid surface due to surfactants and other chemicals coating the bubble, C_B will generally be much closer to 1 than 4.

5.4.3 Effect of the Initial-to-Critical Film Thickness

The ratio of initial-to-critical film thickness, h_0/h_{crit}, must also be known to determine P_{asl}, which will influence k_1. Schulze [1991, 1992] has specified two different equations for h_{crit}, which are functions of surface tension and contact angle. These equations also appear to be system dependent. Schulze [1993] has also indicated that h_0 is a function of particle diameter, fluid viscosity, particle settling velocity, surface tension, and surface mobility, and this function depends on the particular system of interest. Rulev and Dukhin [1986] concluded that both h_0 and h_{crit} are functions of the surface tension and collision process.

They determined that for quasi-elastic collisions ($St > 1$), $h_0/h_{crit} \approx 3$, and for inelastic collisions ($0.1 < St \leq 1$), $h_0/h_{crit} \approx 4$. Therefore, although the specific values of h_0 and h_{crit} are system dependent, the ratio h_0/h_{crit} is typically on the order of 3 to 4 for mineral flotation systems. Since mineral flotation and flotation deinking are assumed to follow similar microprocesses [Heindel, 1999], we assume that h_0/h_{crit} for flotation deinking systems is also within this range.

Figure 16 shows how h_0/h_{crit} influences k_1 for $2 \leq h_0/h_{crit} \leq 5$. In this range, k_1 varies by two orders of magnitude. This parameter is probably one that has a significant influence on the theoretical k_1 value. However, with limited information available in the literature, it can only be assumed to be similar to mineral flotation and range from 3 to 4. This range produces a variation in k_1 by a factor of 5.

6 CONCLUSIONS

This report summarized the current state of the flotation model and provided updates to the bubble/particle attachment and detachment frequencies. The model was then extended to a semi-batch flotation process for model validation. Flotation deinking experiments were then performed in a laboratory flotation cell to validate the flotation model.

The current experimental results did not match the theoretical flotation efficiency predictions very well. It was determined that improvements in the experimental procedures, as well as enhancements in the model will decrease the discrepancy between the predictions and experimental results. We are currently implementing these improvements.

7 FUTURE WORK

The current focus of the flotation modeling aspect of this project addresses the experimental and theoretical improvements alluded to above. Procedures are currently being developed to improve the quality of the experimental data. This will involve the use of a Wemco flotation cell (Fig. 13) and a new image analysis system recently acquired by IPST.

Improvements to the theoretical model are also being made. These involve allowing the bubble to carry more than one particle which is a much more realistic process.

8 NOMENCLATURE LIST

A_c - flotation column cross-sectional area

Bo' - modified Bond number

C_1 - constant

C_B - parameter characterizing bubble surface mobility

D_I - impeller diameter

dP - (differential) probability distribution

dP_U - differential probability distribution for motion in the x-direction

dP_V - differential probability distribution for motion in the y-direction

dP_W - differential probability distribution for motion in the z-direction

dU_i - differential increment in the x component of the velocity field

dU_p - unidirectional particle velocity differential

dV_i - differential increment in the y component of the velocity field

dW_i - differential increment in the z component of the velocity field

d_p - particle diameter

d_{12} - $R_1 + R_2$

E - n_B/n_{po}^f

$E(k,t)$ - energy spectrum

$erf(x)$ - standard error function

f - fluid flow friction factor

$f_{\bar{\lambda}}$ - flow disruption frequency

G - dimensionless particle settling velocity

$\overline{G}$ - velocity gradient perpendicular to the direction of particle motion

g - acceleration due to gravity

$g(r)$ - radial velocity (intermediate flow)

H - height of the flotation column

h_{crit} - critical film thickness

h_0 - initial film thickness

K_1 - empirical turbulence constant

k - wavelength $(1/\bar{\lambda})$

k_* - empirical turbulence constant

k_1 - forward rate constant (attachment)

k_2 - reverse rate constant (detachment)

$k(r)$ - tangential velocity (intermediate flow)

$\tilde{k}_1$ - dimensionless forward rate constant $(k_1 t^* n_{po}^f)$

$\tilde{k}_2$ - dimensionless backward rate constant $(k_2 t^*)$

L - macroscale of turbulence

N_B - total number of bubbles in the column at any time

$\dot{N}_B$ - number of air bubbles entering the column/time

N_I - impeller rotational speed

N_i - number of particles of species i per unit volume

n_B - (constant) concentration of air bubbles

n_B^a - concentration of bubbles with particles attached to them

n_B^f - concentration of free bubbles

n_p - total number of particles/volume

n_p^a - number of particles/volume attached to bubbles

n_p^f - number of free particles/volume

n_{po}^f - initial concentration of free particles

$\mathcal{O}$ - order symbol

P_{asl} - probability of adhesion by sliding

P_c - probability of collision between a particle and a bubble

P_{destab} - probability of destabilization of a bubble/particle aggregate

P_{stab} - probability of stability of a bubble/particle aggregate

P_{tpc} - probability of three phase contact

Q - volumetric air flow rate

R_B - bubble radius

Re_B - bubble Reynolds number

Re_B^* - $\frac{1}{15} Re_B^{0.72}$

Re_p - particle Reynolds number

R_i - radius of i^{th} species

R_p - particle radius

t - time

t^* - bubble residence time

$\tilde{t}$ - dimensionless time

$\overline{U}$ - mean fluid velocity deviation

$\overline{U}_B$ - relative bubble velocity

U_i - x component of the velocity field of the i^{th} species

$\overline{U}_i$ - velocity distribution variance for the i^{th} species

U_p - unidirectional particle velocity

$\overline{U}_p^2$ - variance of a unidirectional particle velocity distribution

V - mixture volume (stock and gas)

V_B - volume of an individual bubble

V_i - y component of the velocity field of the i^{th} species

$\mathcal{V}_{12}$ - relative velocity between particles of species 1 and 2

v_B - bubble rise velocity

v_g - superficial gas velocity

$\boldsymbol{v}_p$ - particle velocity

v_{ps} - particle settling velocity

W_i - z component of the velocity field of the i^{th} species

W_{t_i} - terminal velocity of the i^{th} species

Z - collision frequency between particles and bubbles

Z' - detachment frequency of particles from bubbles

α - dimensionless (total) particle concentration (n_p/n_{po}^f)

$\alpha_i(\tilde{t})$ - i^{th} coefficient in the perturbation expansion of $\alpha(\tilde{t})$

$\Delta\rho_B$ - density difference $(\rho_B - \rho_\ell)$

$\Delta\rho_p$ - density difference $(\rho_p - \rho_\ell)$

ϵ - (Kolmogorov) turbulent energy density (or dissipation rate)

ϵ_p - gas holdup per unit volume $(V_B n_B)$

η - microscale of turbulence

γ - dimensionless (free) particle concentration (n_p^f/n_{po}^f)

$\gamma_i(\tilde{t})$ - i^{th} coefficient in the perturbation expansion of $\gamma(\tilde{t})$

λ - dimensionless friction factor

$\overline{\lambda}$ - eddy scale comparable with an aggregate diameter

μ_ℓ - fluid dynamic viscosity

ν_ℓ - kinematic viscosity

ρ_B - bubble (gas) density

ρ_ℓ - fluid density

ρ_p - particle density

σ - surface tension

θ - contact angle

9 REFERENCES

1. Abrahamson, J., "Collision Rates of Small Particles in a Vigoroulsy Turbulent Fluid," *Chem Eng. Sci.,* **30**, 1975, 1371-1379.

2. Batchelor, G.K., *The Theory of Homogeneous Turbulence*, Cambridge University Press, Cambridge, U.K., 1953.

3. Bloom, F. and Heindel, T.J., "Mathematical Modelling of the Flotation Deinking Process," *Mathl. Comput. Modelling,* **25**, 1997a, 13-58.

4. Bloom, F. and Heindel, T.J., "A Theoretical Model of Flotation Deinking Efficiency," *J. Colloid and Interface Sci.,* **190**, 1997b, 182-197.

5. Camp, T.R., and Stein, P.C., "Velocity Gradients and Internal Work in Fluid Motion," *J. Boston Soc., Civil Engrs.,* **30**, 1943, 219-237.

6. Heindel, T.J., "A Method to Visualize Gas Bubbles in a Pulp Suspension," Project F00903 Report 3, IPST Member Company Report (February 1997).

7. Heindel, T.J., "Fundamentals of Flotation Deinking," *TAPPI Journal*, **82**(3): 115-124 (1999).

8. Heindel, T.J., and Bloom, F., "Mathematical Modeling of the Overall Flotation Deinking Process," Project F00903 Report 1, IPST Member Company Report (December 1995).

9. Heindel, T.J., and Bloom, F., "Mathematical Modeling of the Overall Flotation Deinking Process: Predictions of Selected Performance Parameters," Project F00903 Report 2, IPST Member Company Report (November 1996).

10. Heindel, T.J., and Bloom, F., "Mathematical Modeling of the Overall Flotation Deinking Process: Probability of Collision Improvements," Project F00903 Report 4, IPST Member Company Report (January 1998a).

11. Heindel, T.J., and Bloom, F., "Mathematical Modeling of the Overall Flotation Deinking Process: Probability of Attachment by Sliding Improvements," Project F00903 Report 6, IPST Member Company Report (May 1998b).

12. Heindel, T.J., and Emery, A.E., "The Effect of ONP Chemistry and Fiber Type on Gas Bubble Size in a Quiescent Bubble Column," Project F00903 Report 5, IPST Member Company Report (February 1998).

13. Heindel, T.J., and Garner, A.E., "Bubble Size Measurements in a Cocurrent Bubble Column Filled with Various Consistencies of Copy Paper," Project F00903 Report 8, IPST Member Company Report (March 1999).

14. Hinze, J.O., *Turbulence*, McGraw Hill Pub., New York, 1959.

15. Johnson, D.A., and Thompson, E.V., "Fiber and Toner Detachment During Repulping of Mixed Office Waste Containing Photocopied and Laser-Printed Paper," *Tappi J.*, **78**(2): 41-46 (1995).

16. Liepe, F. and Möckel, O.H., "Untersuchungen zum Stoffvereinigen in flüssiger Phase," *Chem Techn.*, **28**, 1976, 205-209.

17. Maruvada, K.S., and Heindel, T.J., "A Methodology for Flotation Deinking Model Validation," Project F00903 Report 7, IPST Member Company Report (July 1998).

18. Mika, T.S. and Fuerstenau, D.W., "A Microscopic Model of the Flotation Process," in *Proc. of the 8th Int. Mineral Processing Congress*, Leningrad, 1968, 246-269.

19. Pan, R., Johnson, D.A., and Thompson, E.V., "Fiber/Toner Detachment Studies: Repulping and Flotation of Laser Printed Paper. Part II," *1995 TAPPI Recycling Symposium*, TAPPI Press, Atlanta, GA, 37-45 (1995).

20. Parker, D.S., Kaufman, W.J., and D. Jenkins, "Floc Breakup in Turbulent Flocculation Processes," *J. Sanit. Eng. Div., Proc. Am. Soc. Civil Eng.*, **98**, 1972, 79-99.

21. Rulev, N.N., and Dukhin, S.S., "Dynamics of the Thinning of the Film of Liquid Formed Upon the Inertial Impact of a Spherical Particle on the Surface of a Bubble," *Kolloidnyi Zhurnal*, **48**: 302-310 (1986).

22. Saffman, P.G. and Turner, T.S., "On the Collision of Drops in Turbulent Clouds," *J. Fluid Mech.*, **1**, 1956, 16-30.

23. Schubert, H. and C. Bisehofberger, "On the Optimization of Hydrodynamics in Flotation Processes," in *Mineral Processing, Proc. 13th Int. Mineral Processing Congress*, J. Laskowski, ed., Elsevier, Warsaw, 1981, 1261-1284.

24. Schulze, H.J., "The Fundamentals of Flotation Deinking in Comparison to Mineral Flotation," *1st Research Forum on Recycling*, CPPA Press, Toronto, 161-167 (1991).

25. Schulze, H.J., "Probability of Particle Attachment on Gas Bubbles by Sliding," *Advances in Colloid and Interface Science*, **40**: 283-305 (1992).

26. Schulze, H.J., "Flotation as a Heterocoagulation Process: Possibilities of Calculating the Probability of Flotation," in *Coagulation and Flocculation*, B. Dobias, Ed., 321-353 (1993).

27. Schulze, H.J., "Hydrodynamik der Flotations - Elementarvorgänge," *Wochen blatt für Paperfabrikation*, **122**, (1994), 160-168.

28. Smoluchowski, M., *Z. Phys. Chem*, 92, 1917, 129.

29. Thomas, D.G., "Turbulent Disruption of Flocs in Small Particle Size Suspensions," *A.I.Ch.E Journal*, **10**, 1964, 517-523.

30. Thompson, E.V., Review of Flotation Research by the Cooperative Recycled Fiber Studies Program, Department of Chemical Engineering, University of Maine," in *Paper Recycling Challenge: Vol. 2 Deinking and Bleaching*, M.R. Doshi and J.M. Dyer, Eds., Doshi & Associates, Inc., Appleton, WI, 31-68 (1997).

31. Vidotti, R.M., Johnson, D.A., and Thompson, E.V., "Hydrodynamic Particle Volume and Its Relationship to Mixed Office Waste Paper Flotation Efficiency, Part I," *1995 TAPPI Pulping Conference*, TAPPI Press, Atlanta, GA, 203-213 (1995a).

32. Vidotti, R.M., Johnson, D.A., and Thompson, E.V., "Influence of Toner Detachment During Mixed Office Waste Paper Repulping on Flotation Efficiency," *3rd Research Forum on Recycling*, Vancouver, BC, CPPA Press, 257- 268 (November 20-22, 1995b).

33. Vidotti, R.M., Johnson, D.A., and Thompson, E.V., "Visual Observations of Bubble/Particle Interactions," *4th Research Forum on Recycling*, Chteau Frontenac, Qubec, CPPA Press, 39-46 (October 7-9, 1997).

34. Wågberg, L. and T. Lindstrom, "Kinetics of Polymer-Induced Flocculation of Cellulosic Fibers in Turbulent Flow," *Colloids and Surfaces,* **27**, 1987, 29-42.

35. Yoon, R.H., and Luttrell, G.H., "The Effect of Bubble Size on Fine Particle Flotation," in *Mineral Processing and Extractive Metallurgy Review*, **5**, 1989, 101-122.

10 TABLES

Table 1: Experimentally determined k_1 and k_2 values through a "best fit" curve fitting technique.

$R_p(\mu m)$		"best fit" to both k_1 and k_2	"best fit" to k_1 with $k_2 = 0$	"best fit" to k_1 with k_2 determined from (3.7b)
37.5	k_1	3.447×10^{-8}	3.447×10^{-8}	3.449×10^{-8}
	k_2	-5.067×10^{-5}	0	4.818×10^{-4}
	R^2	0.91	0.91	0.91
62.5	k_1	3.393×10^{-8}	3.395×10^{-8}	4.136×10^{-8}
	k_2	-4.754×10^{-4}	0	1.447×10^{-1}
	R^2	0.87	0.87	0.87
87.5	k_1	3.151×10^{-8}	3.152×10^{-8}	-1.394×10^{-8}
	k_2	-3.616×10^{-4}	0	1.645×10^{0}
	R^2	0.96	0.96	0.80
112.5	k_1	3.578×10^{-8}	3.587×10^{-8}	-3.276×10^{-9}
	k_2	-1.811×10^{-3}	0	6.285×10^{0}
	R^2	0.90	0.90	0.72

Tables 2: Theoretical k_1 and k_2 values.

$R_p(\mu m)$	k_1	k_2
37.5	6.673×10^{-10}	4.818×10^{-4}
62.5	2.001×10^{-9}	1.447×10^{-1}
87.5	4.137×10^{-9}	1.645×10^{0}
112.5	6.971×10^{-9}	6.285×10^{0}

Table 3: Conditions for the parametric evaluations in Section 5.4.

R_p	62.5μm
ρ_p	1.2 g/cm^3
R_B	0.5 mm
$R_{B,\max}$	1.0 mm
ρ_1	1 g/cm^3
θ	60°
C_B	1
σ	35 dynes/cm
h_0/h_{crit}	3

11 FIGURES

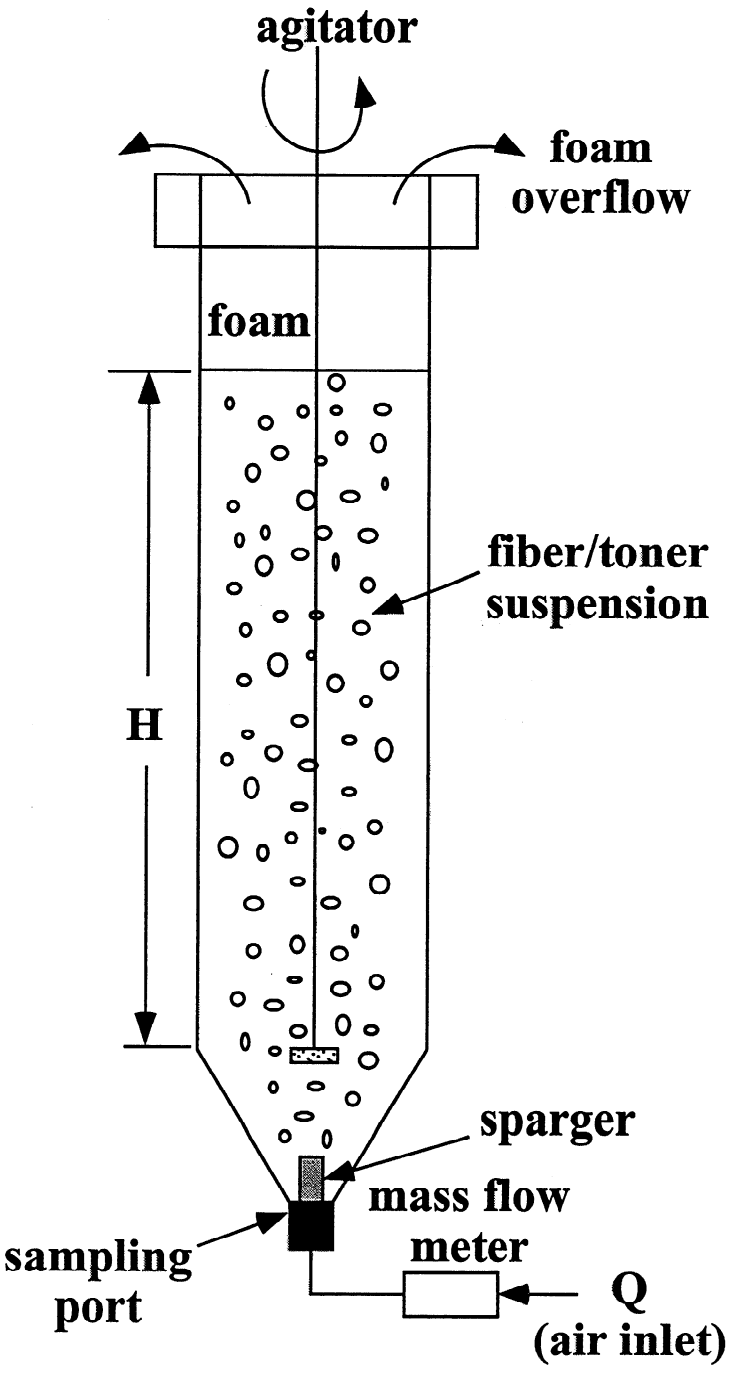

Figure 1: Schematic of the laboratory flotation cell used in this study.

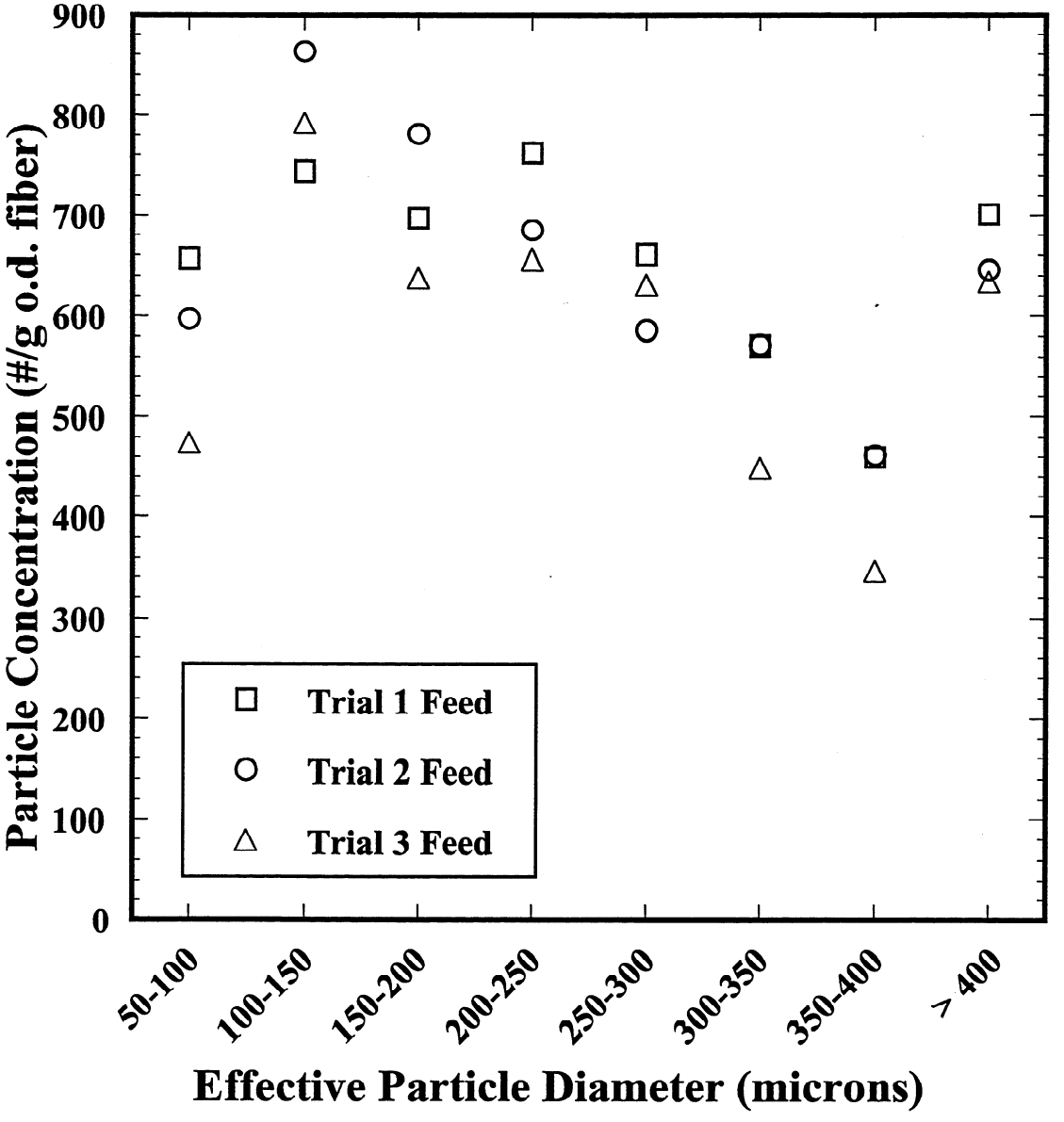

Figure 2: Particle concentration distribution of the flotation feed streams.

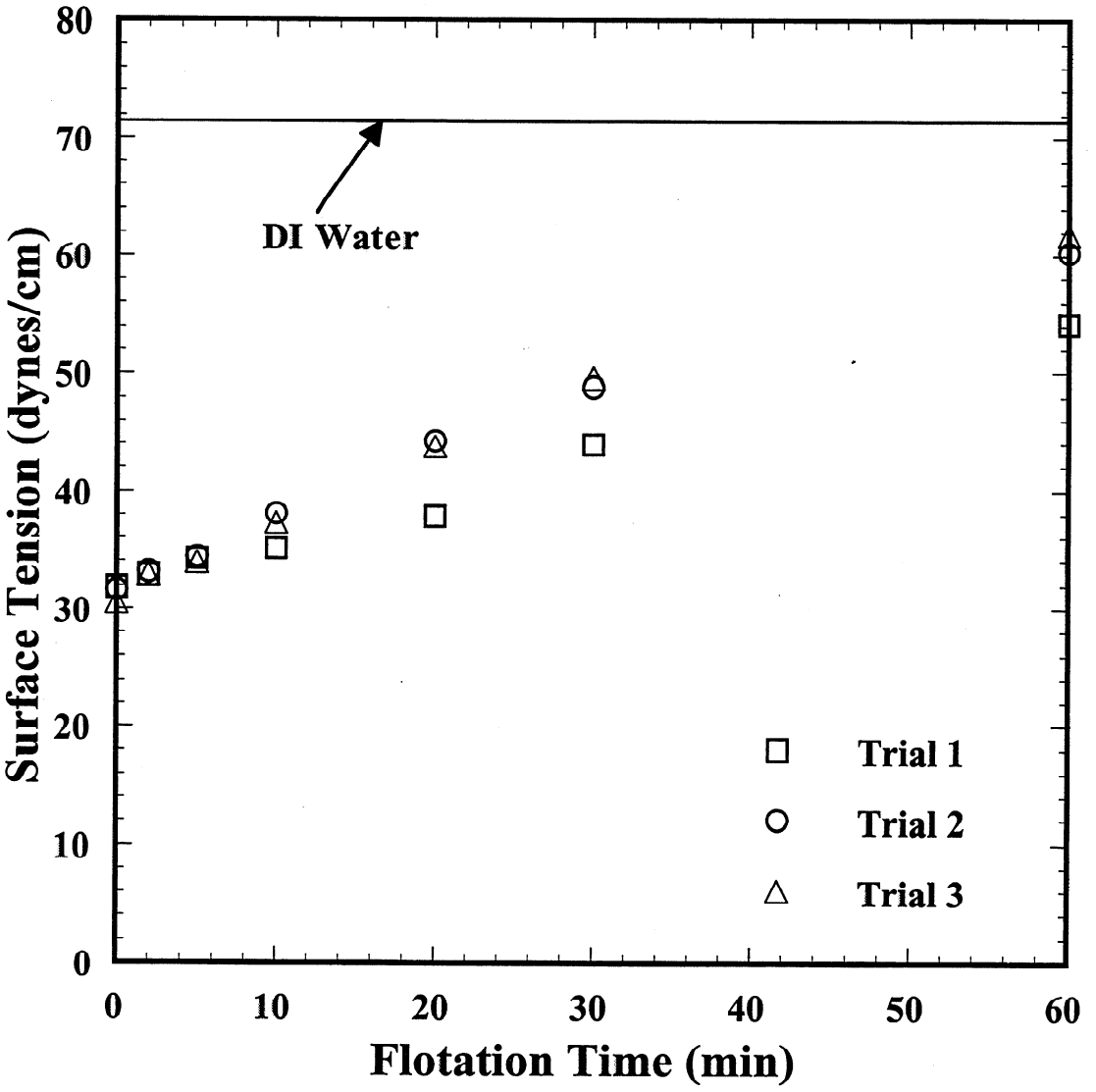

Figure 3: Surface tension variation as a function of flotation time.

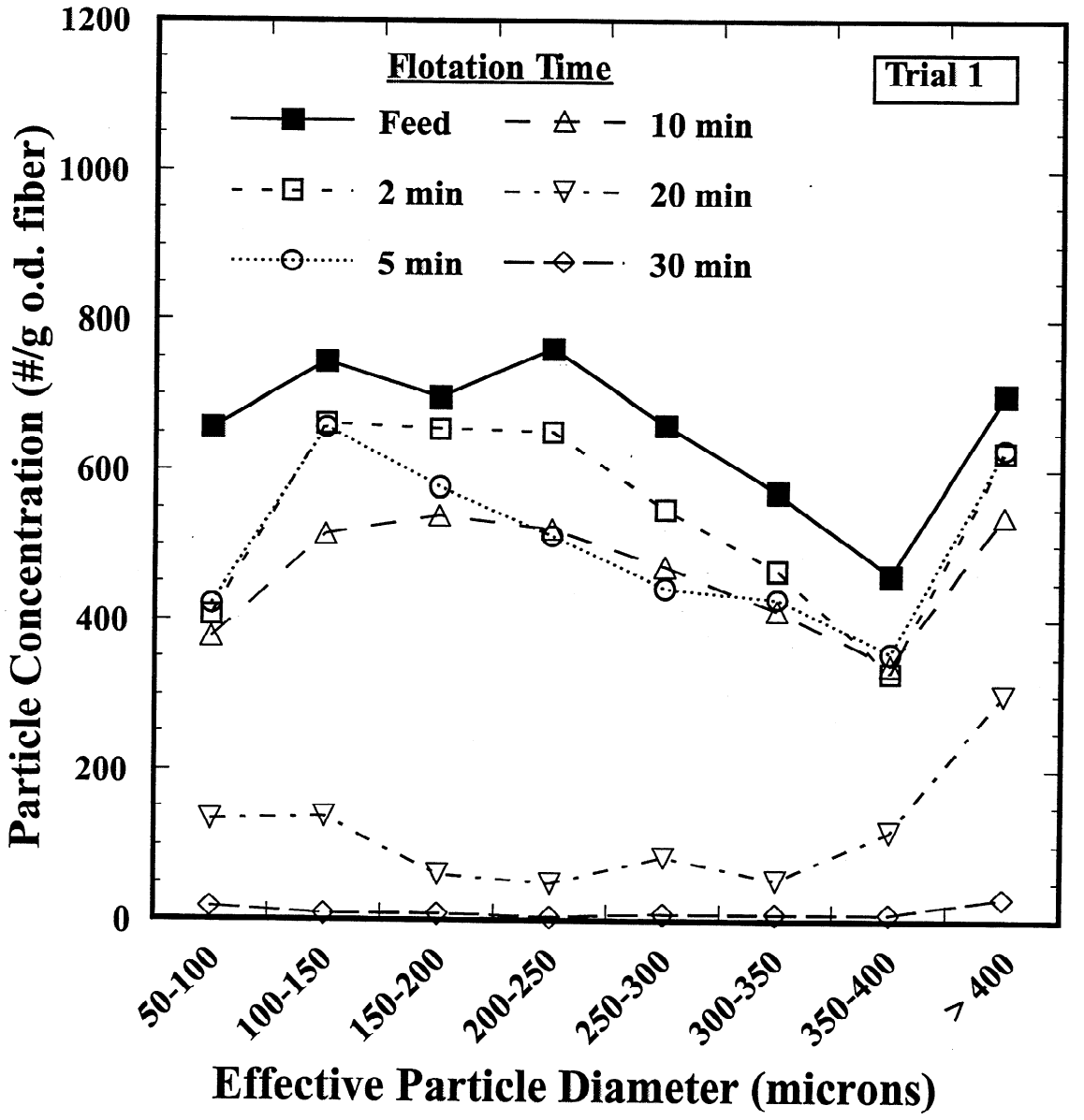

Figure 4: Particle concentrations for various Trial 1 flotation times.

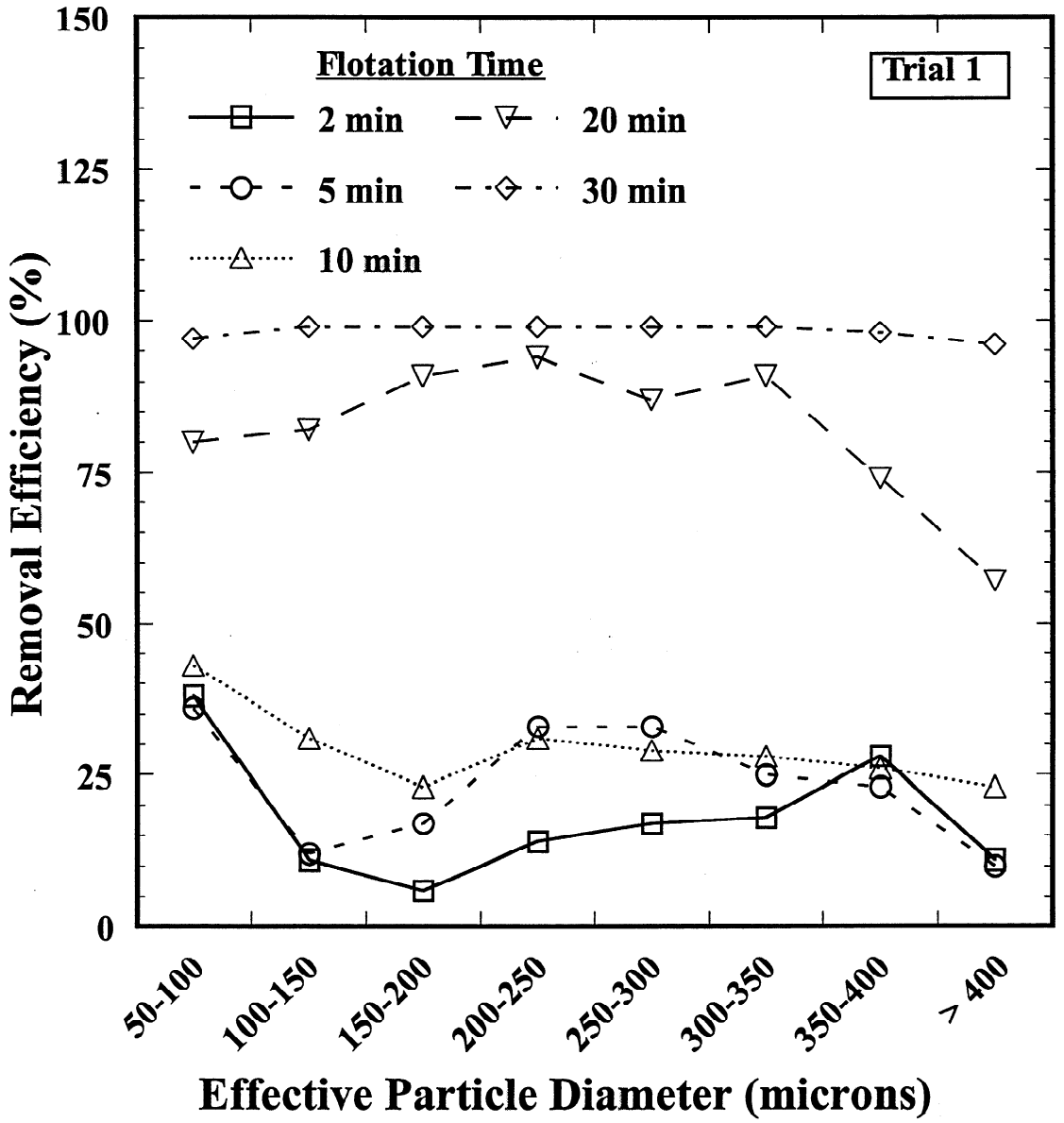

Figure 5: Particle removal efficiency for various Trial 1 flotation times.

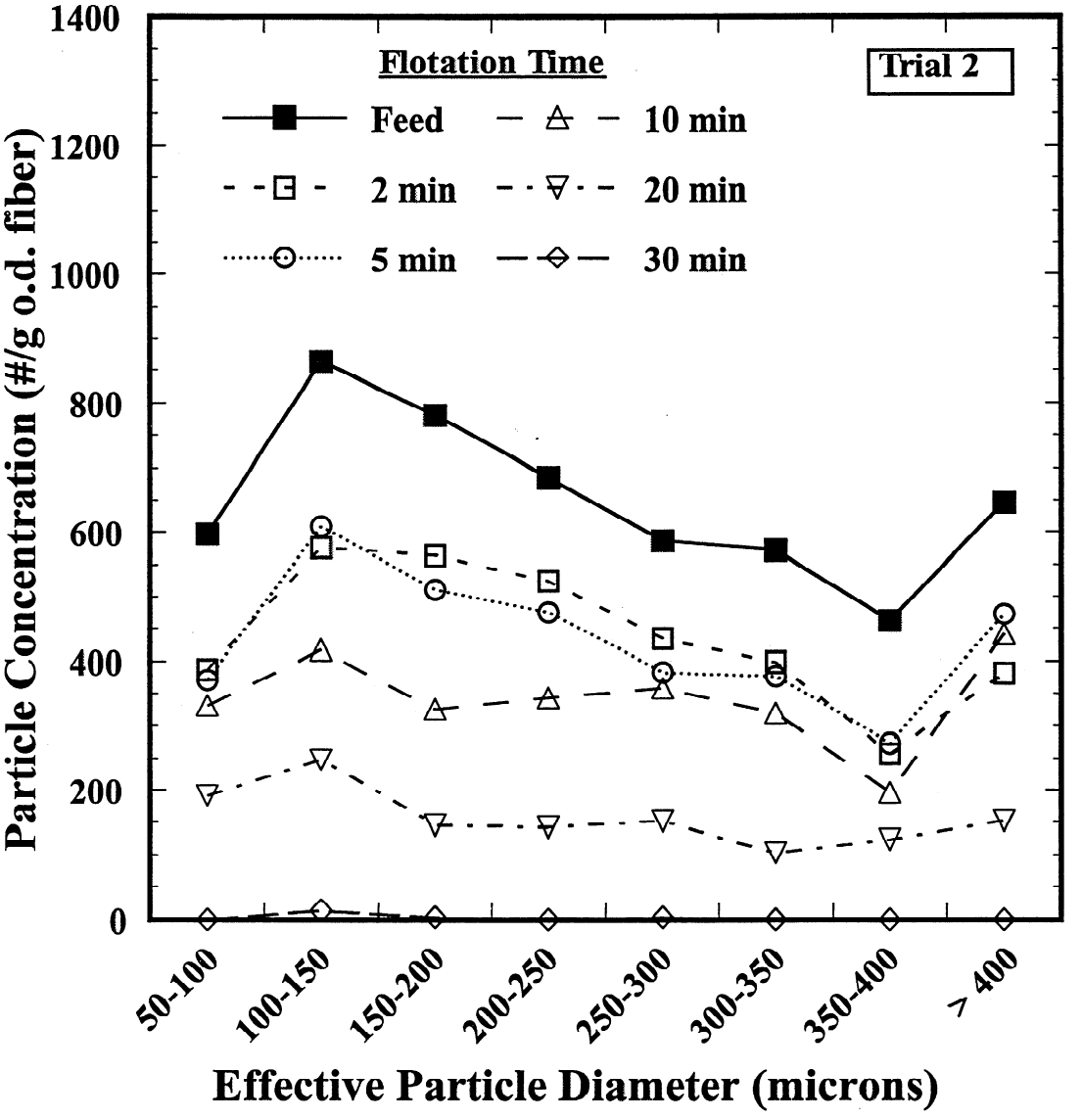

Figure 6: Particle concentrations for various Trial 2 flotation times.

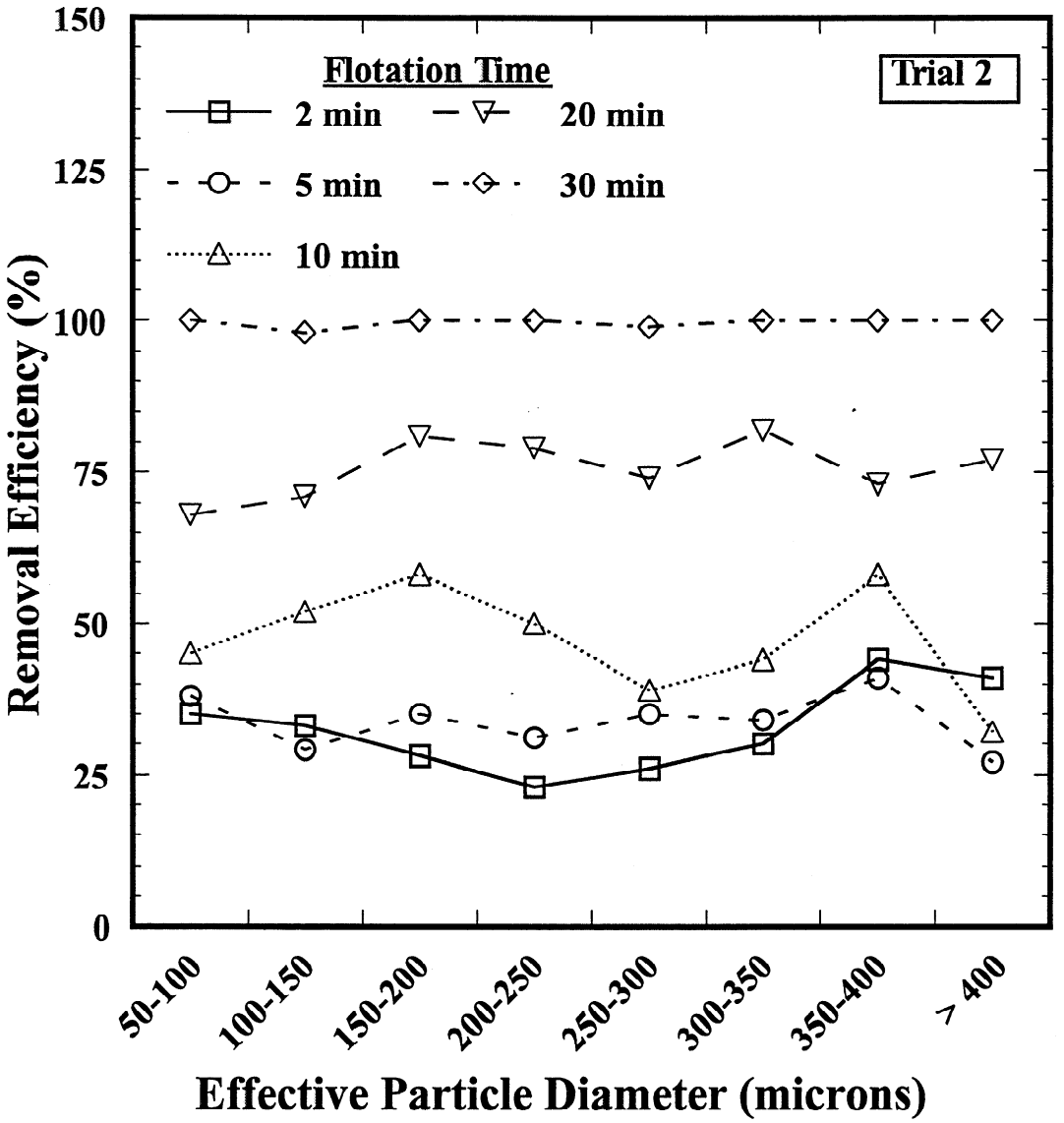

Figure 7: Particle removal efficiency for various Trial 2 flotation times.

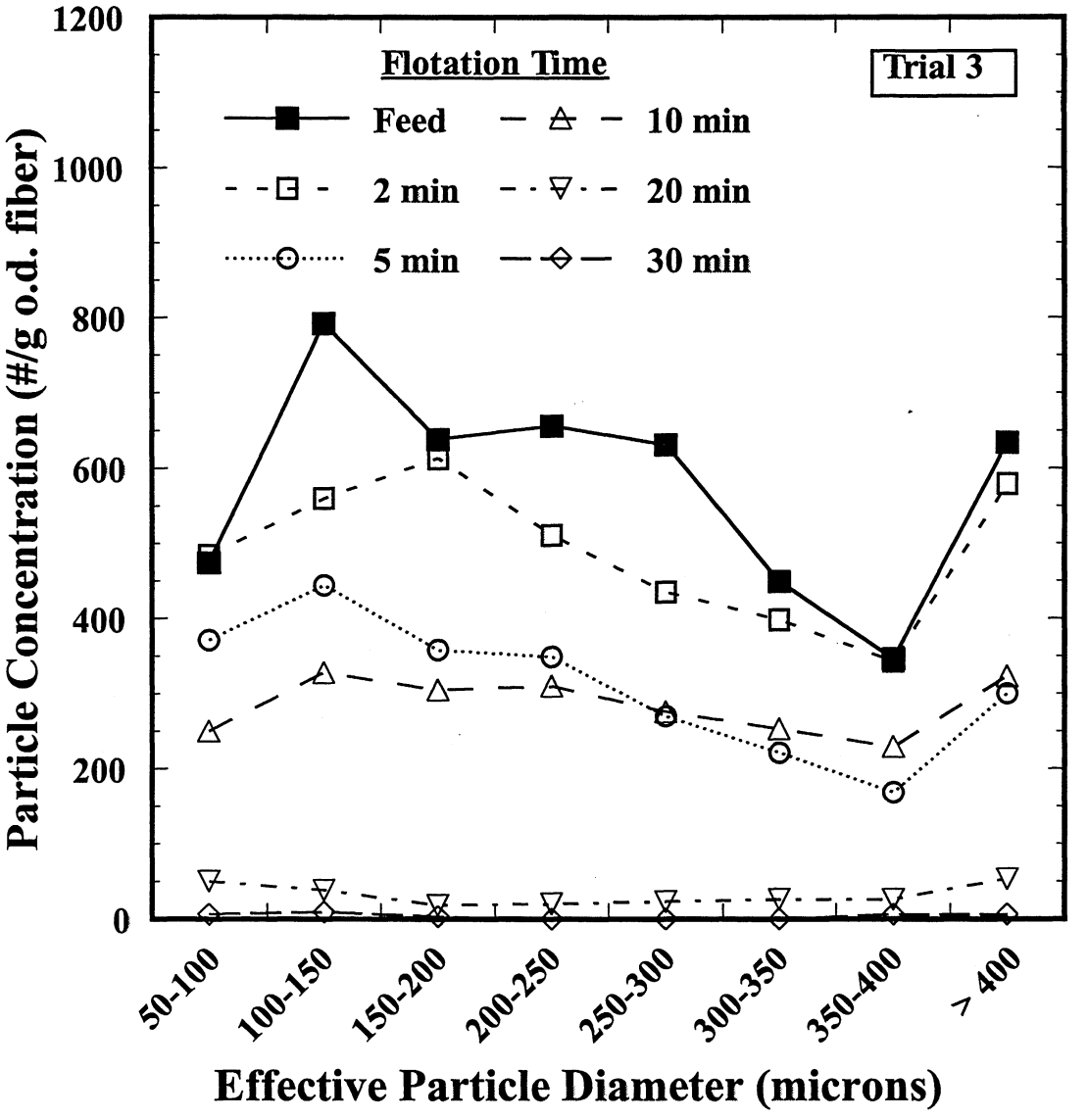

Figure 8: Particle concentrations for various Trial 3 flotation times.

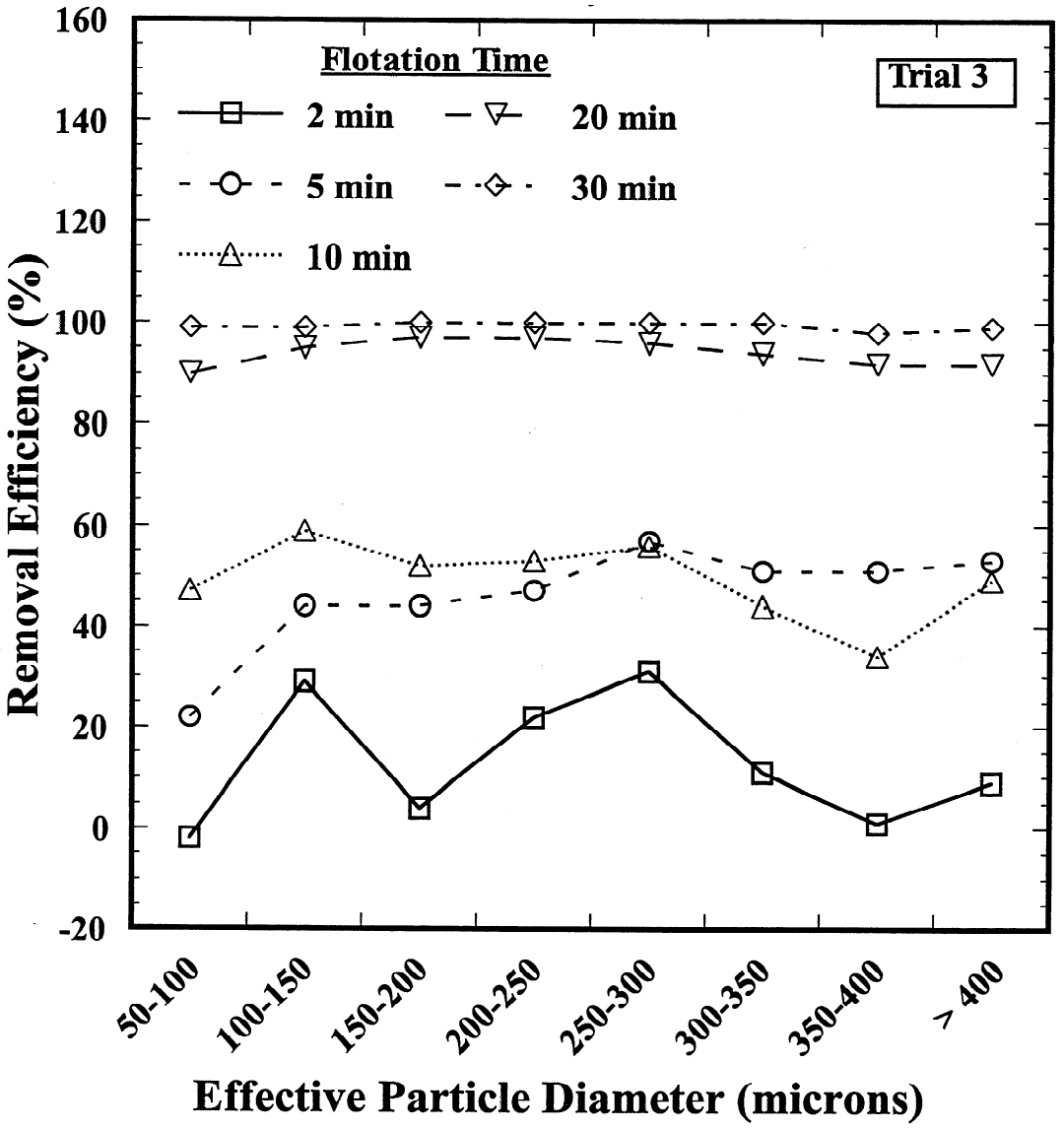

Figure 9: Particle removal efficiency for various Trial 3 flotation times.

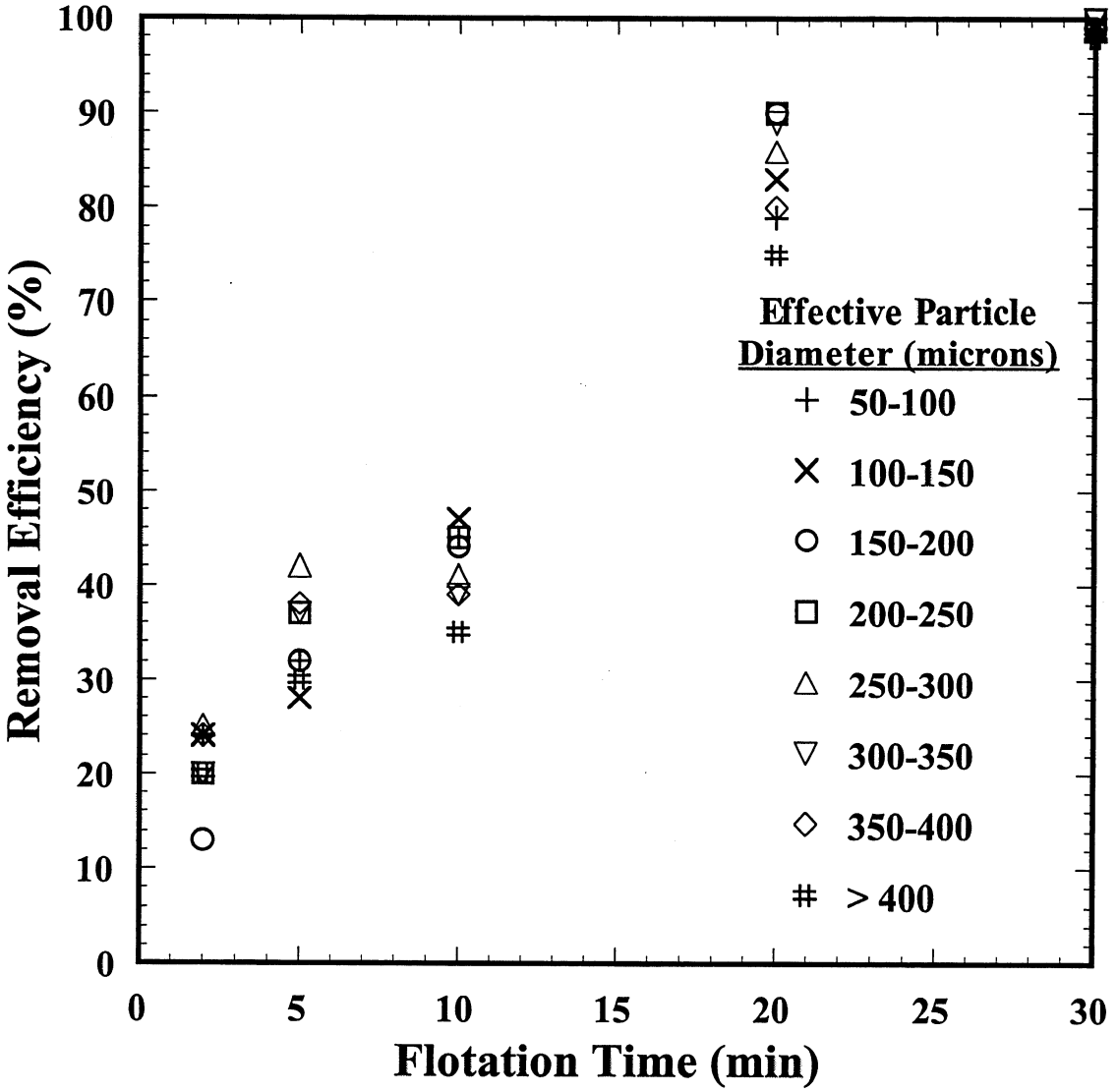

Figure 10: Average removal efficiency as a function of flotation time for different particle size ranges.

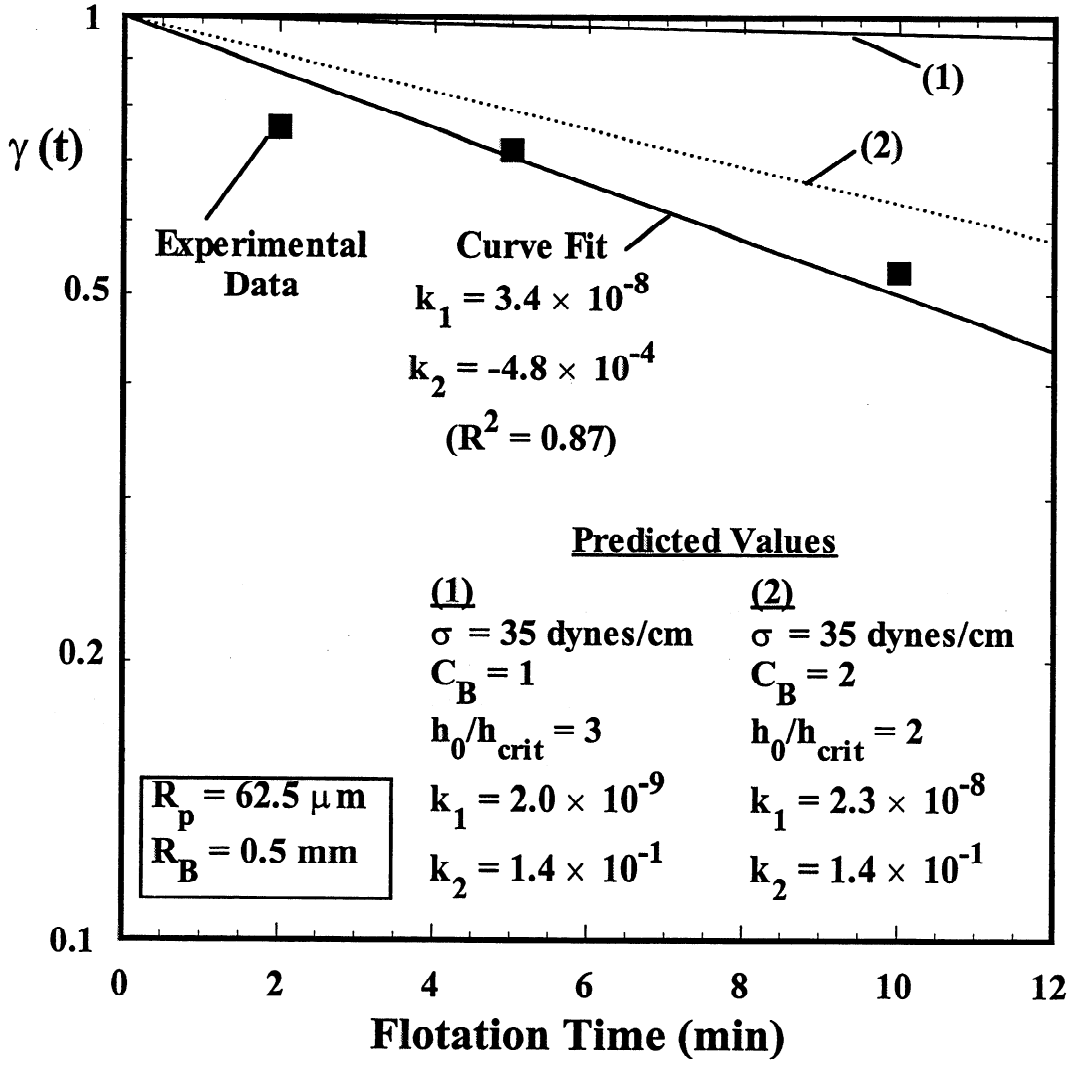

Figure 11: Experimental and theoretical $\gamma(t)$ for $R_p = 62.5\mu$m and $R_B = 0.5$ mm.

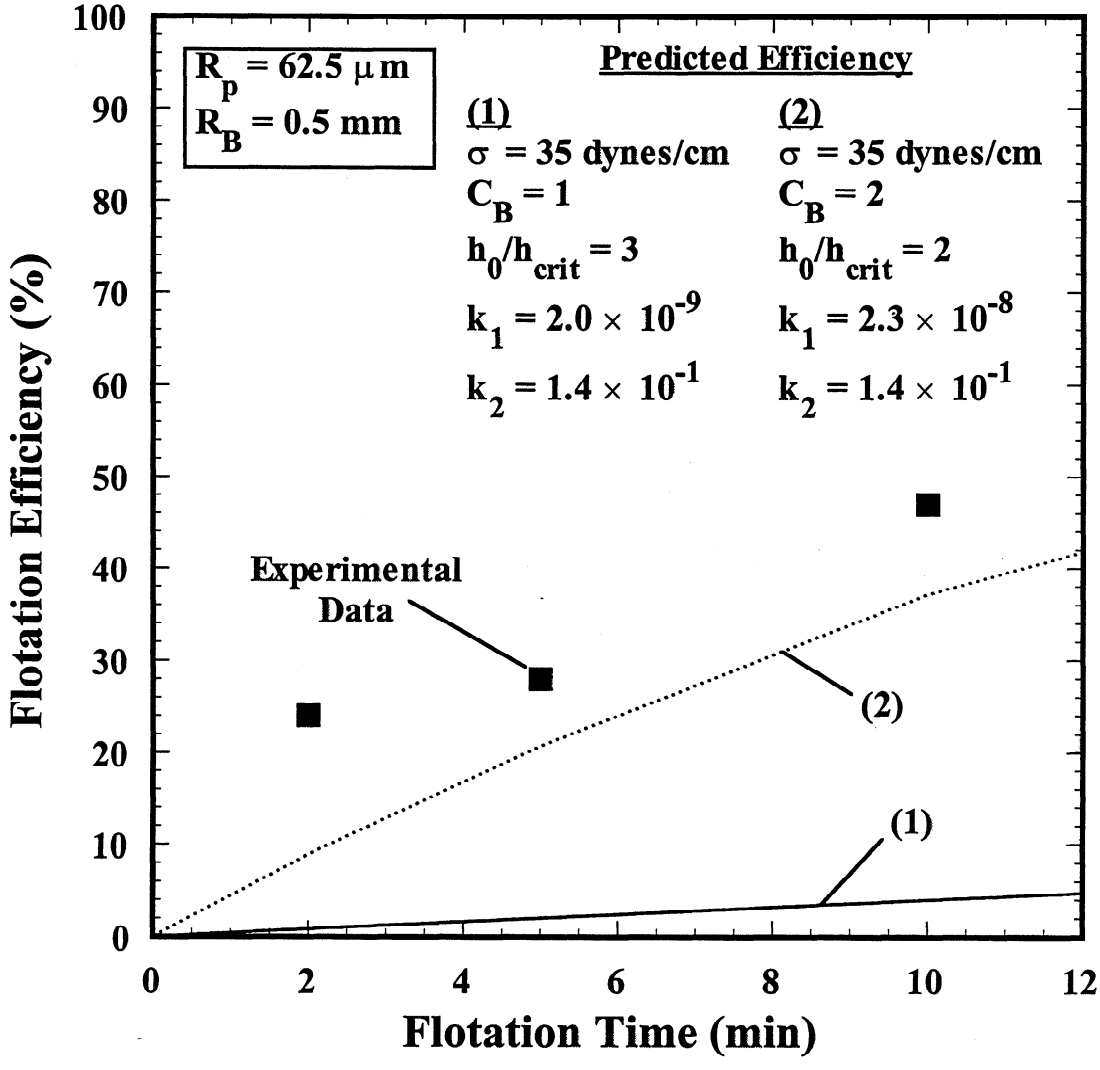

Figure 12: Experimental and theoretical flotation removal efficiency for R_p = 62.5 μm and R_B = 0.5 mm.

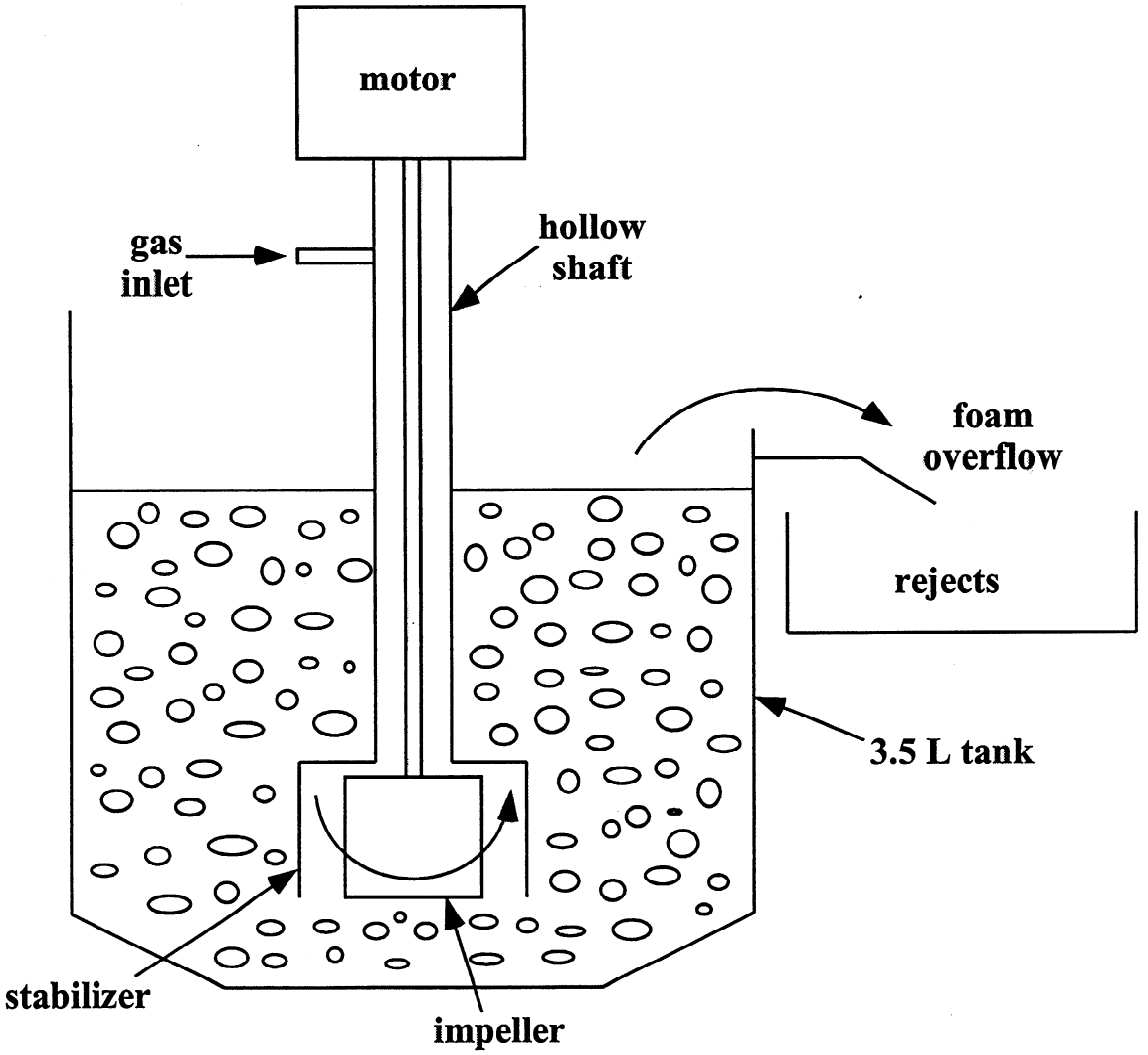

Figure 13: Laboratory Wemco flotation cell schematic.

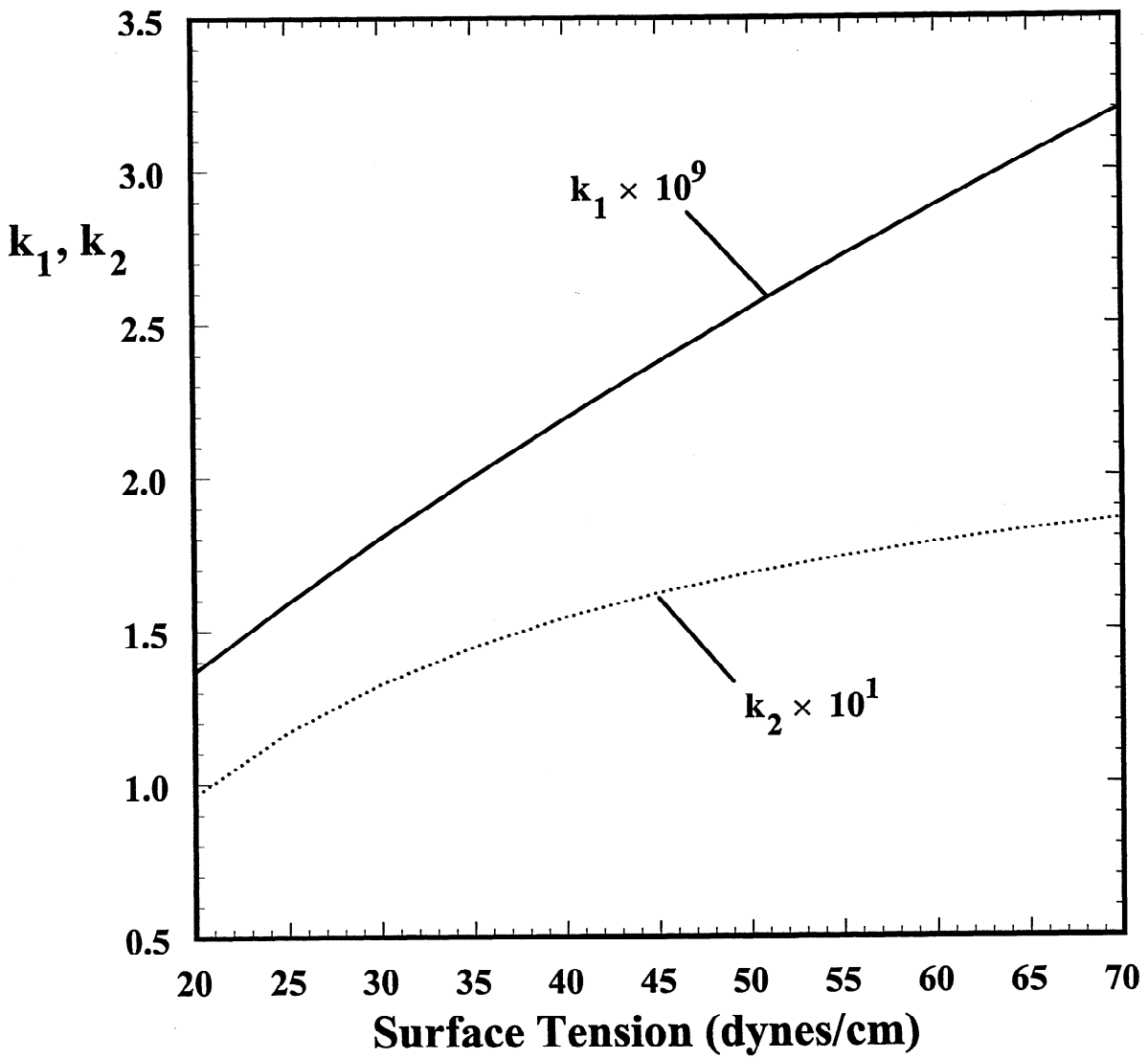

Figure 14: The effect of surface tension on k_1 and k_2.

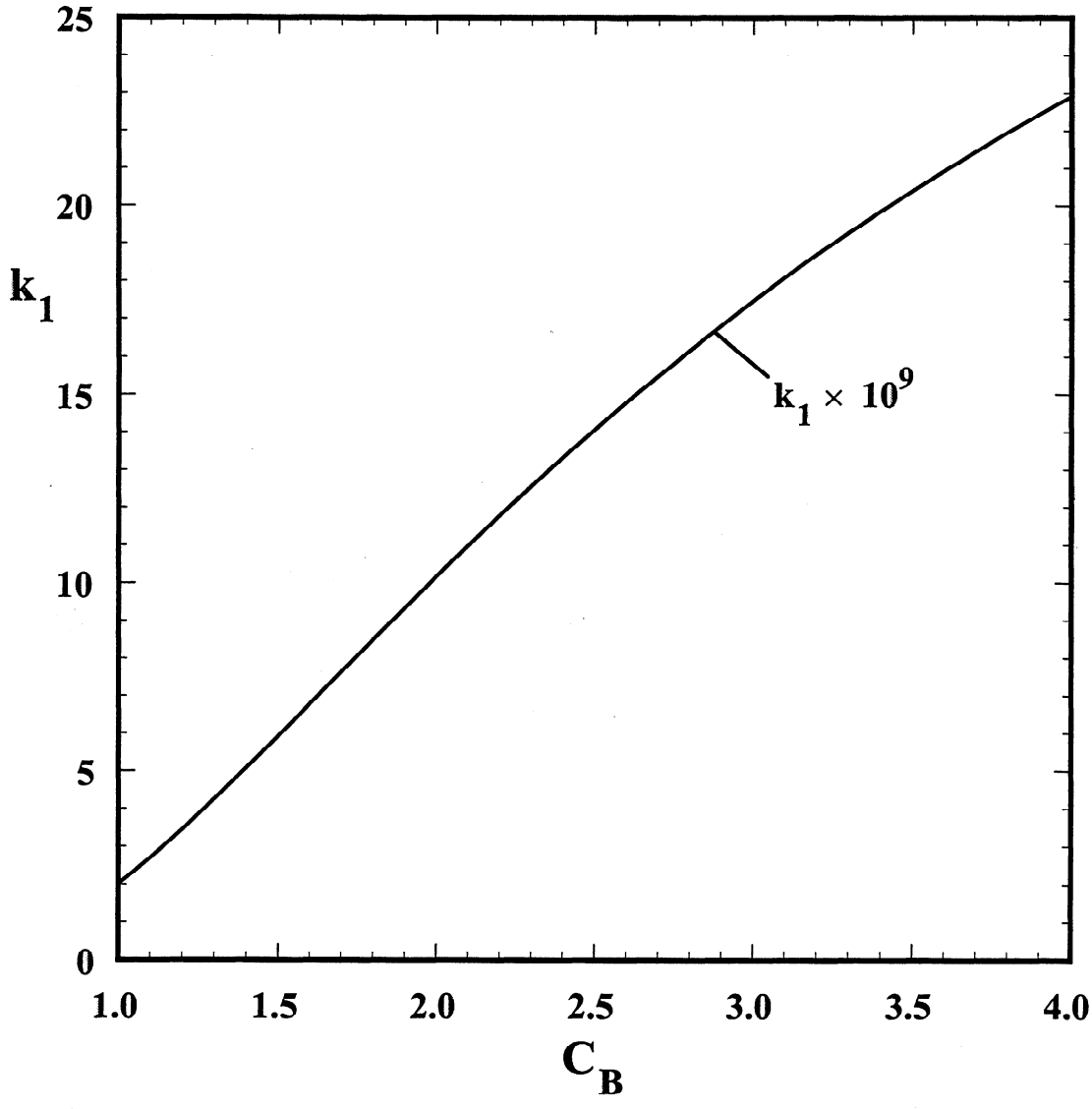

Figure 15: The effect of the surface mobility coefficient on k_1.

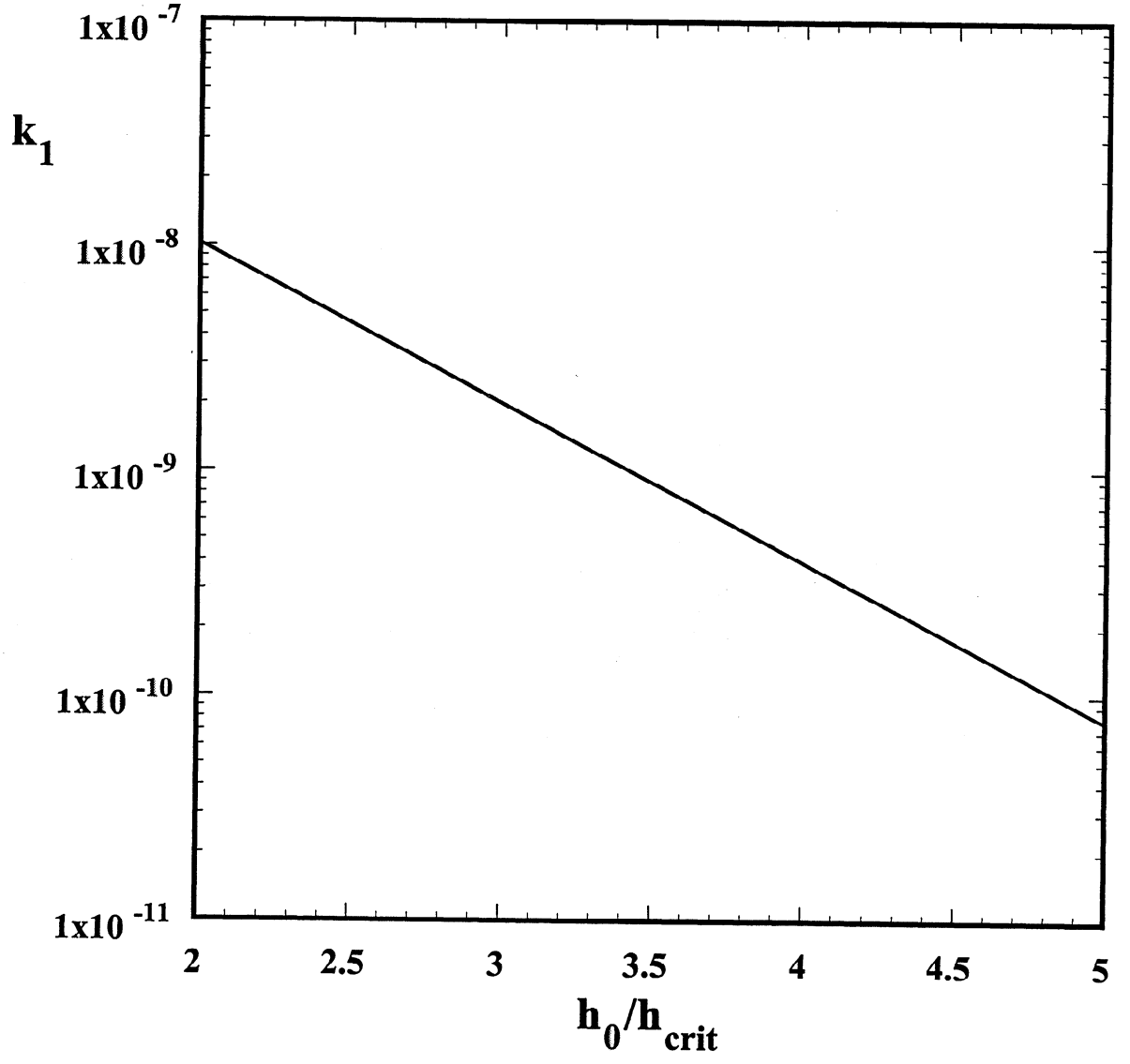

Figure 16: The effect of the critical-to-initial film thickness ratio on k_1.

12 APPENDIX

Table A.1: Experimental flotation efficiency summary.

Particle Size Range	Trial	Flotation Time (minutes)					
		2	5	10	20	30	60
50-100 μm	Trial 1	38	36	43	80	97	95
	Trial 2	35	38	45	68	100	100
	Trial 3	-2	22	47	90	99	99
	Average	24	32	45	79	99	98
100-150μm	Trial 1	11	12	31	82	99	97
	Trial 2	33	29	52	71	98	100
	Trial 3	29	44	59	95	99	100
	Average	24	28	47	83	99	99
150-200μm	Trial 1	6	17	23	91	99	100
	Trial 2	28	35	58	81	100	99
	Trial 3	4	44	52	97	100	99
	Average	12	32	44	90	100	99
200-250μm	Trial 1	14	33	31	94	99	100
	Trial 2	23	31	50	79	100	100
	Trial 3	22	47	53	97	100	100
	Average	20	37	45	90	100	100
250-300μm	Trial 1	17	33	29	87	99	100
	Trial 2	26	35	39	74	99	100
	Trial 3	31	57	56	96	100	100
	Average	25	42	41	86	99	100
300-350μm	Trial 1	18	25	28	91	99	99
	Trial 2	30	34	44	82	100	100
	Trial 3	11	51	44	94	100	100
	Average	20	37	39	89	100	100
350-400μm	Trial 1	28	23	26	74	98	100
	Trial 2	44	41	58	73	100	100
	Trial 3	1	51	34	92	98	99
	Average	24	38	39	80	99	100
$>$ 400μm	Trial 1	11	10	23	57	96	100
	Trial 2	41	27	32	77	100	100
	Trial 3	9	53	49	92	99	99
	Average	20	30	35	75	98	100
Average	Trial 1	17	23	29	82	98	99
	Trial 2	32	33	48	76	100	100
	Trial 3	15	46	51	95	99	100
	Overall Average	21	34	43	84	99	100